The accretion history of the Milky Way. I. How it shapes globular clusters and dwarf galaxies

Francois Hammer, Hefan Li, Gary A. Mamon, Marcel S. Pawlowski, Piercarlo Bonifacio, Yongjun Jiao, Haifeng Wang, Jianling Wang, Yanbin Yang

▶ **To cite this version:**

Francois Hammer, Hefan Li, Gary A. Mamon, Marcel S. Pawlowski, Piercarlo Bonifacio, et al.. The accretion history of the Milky Way. I. How it shapes globular clusters and dwarf galaxies. Monthly Notices of the Royal Astronomical Society, 2023, 519 (4), pp.5059-5075. 10.1093/mnras/stac3758 . hal-03925275

HAL Id: hal-03925275
https://hal.science/hal-03925275

Submitted on 23 Apr 2024

HAL is a multi-disciplinary open access archive for the deposit and dissemination of scientific research documents, whether they are published or not. The documents may come from teaching and research institutions in France or abroad, or from public or private research centers.

L'archive ouverte pluridisciplinaire **HAL**, est destinée au dépôt et à la diffusion de documents scientifiques de niveau recherche, publiés ou non, émanant des établissements d'enseignement et de recherche français ou étrangers, des laboratoires publics ou privés.

Monthly Notices of the ROYAL ASTRONOMICAL SOCIETY
MNRAS **519,** 5059–5075 (2023) https://doi.org/10.1093/mnras/stac3758

The accretion history of the Milky Way – I. How it shapes globular clusters and dwarf galaxies

Francois Hammer [1]★ Hefan Li,[2,3] Gary A. Mamon [4] Marcel S. Pawlowski,[5] Piercarlo Bonifacio [1] Yongjun Jiao,[1] Haifeng Wang,[1,6] Jianling Wang [3] and Yanbin Yang [1]

[1]*GEPI, Observatoire de Paris, Paris Sciences et Lettres, CNRS, Place Jules Janssen, F-92195 Meudon, France*
[2]*School of Physical Sciences, University of Chinese Academy of Sciences, Beijing 100049, P. R. China*
[3]*CAS Key Laboratory of Optical Astronomy, National Astronomical Observatories, Beijing 100101, China*
[4]*Institut d'Astrophysique de Paris (UMR7095: CNRS & Sorbonne Université), 98 bis Bd Arago, F-75014 Paris, France*
[5]*Leibniz-Institut fuer Astrophysik Potsdam (AIP), An der Sternwarte 16, D-14482 Potsdam Germany*
[6]*CREF, Centro Ricerche Enrico Fermi, Via Panisperna 89A, I-00184 Roma, Italy*

Accepted 2022 December 12. Received 2022 November 30; in original form 2022 September 6

ABSTRACT

Halo inhabitants are individual stars, stellar streams, star, and globular clusters, and dwarf galaxies. Here we compare the two last categories that include objects of similar stellar mass, which are often studied as self-dynamical equilibrium systems. We discover that the half-light radius of globular clusters depends on their orbital pericentre and total energy, and that Milky Way (MW) tides may explain the observed correlation. We also suggest that the accretion epoch of stellar systems in the MW halo can be calibrated by the total orbital energy, and that such a relation is due to both the mass growth of the MW and dynamical friction affecting mostly satellites with numerous orbits. This calibration starts from the bulge to Kraken, *Gaia* Sausage Enceladus, Sagittarius stellar systems, and finally to the new coming dwarfs, either or not linked to the vast-polar structure. The most eccentric globular clusters, and dwarfs have their half-light radius scaling as the inverse of their binding energy, and this over more than two decades. This means that earlier arriving satellites are smaller due to the tidal effects of the MW. Therefore, most halo inhabitants appear to have their structural parameters shaped by MW tides, and also by ram-pressure for the most recent arrivals, the dwarf galaxies. The correlations found in this study can be used as tools to further investigate the origin of globular clusters and dwarfs, as well as the assembly history of our Galaxy.

Key words: Galaxy: evolution – globular clusters: general – Galaxy: halo – galaxies: dwarf – galaxies: interactions.

1 INTRODUCTION

The stellar system content of the Milky Way (MW) halo has been used to determine its merger history, the understanding of which has been considerably improved with the orbital constraints derived from the all-sky *Gaia* EDR3 observations. Since the dynamical probes of the MW gas disc are limited by 20–25 kpc in radial distance, the halo inhabitants are also used as dynamical probes to constraint the mass of our Galaxy at large radii, and ultimately, its total mass.

However, which type of orbital equilibrium with the MW potential has been reached by the halo stellar systems? Are their orbits ruled by the Jeans equation meaning that they can be used to probe the MW mass? Are they at pseudo equilibrium as, e.g. regularly affected by tidal shocks such as globular clusters (GCs) when passing near the inner bulge, or when crossing the disc (Aguilar, Hut & Ostriker 1988; Gnedin & Ostriker 1999)? Alternatively, could some of them be near their first pericentric passage having recently lost their gas and being mostly out of equilibrium (Yang et al. 2014)? Comparative studies of their orbits could bring some answers to these questions.

Thanks to the *Gaia* astrometric mission, considerable efforts have been made to reveal the history of the ancient merger events having affected the Milky Way (Kruijssen et al. 2019, 2020; Massari, Koppelman & Helmi 2019; Malhan et al. 2022). This has generated a large variety of events often nicknamed on the basis of various mythologies. Perhaps, the most achieved effort to date has been made by Malhan et al. (2022) who used specific search tools that compares angular momenta, total energy of 170 globular clusters, 41 stellar streams, and 46 dwarf galaxies, providing some homogeneity in characterizing previous events. Apart from Sagittarius (Sgr) and Willman I, their classification of ancient mergers does not include dwarf galaxies, which are likely newcomers due to their considerably higher energy and angular momentum (Hammer et al. 2021).

Section 2 presents the data from *Gaia* EDR3, and indicates how they have been analysed to produce orbital quantities, and it is accompanied by Appendix C containing the result for GCs. Section 3 reveals the strong correlation between intrinsic ($r_{\rm half}$) and orbital ($R_{\rm peri}$) parameters, and provides an interpretation of its origin. Section 4 suggests that the epoch of infall of stellar systems in the MW halo can be approximated by the total energy, which is discussed and explained in Section 5.1 and implies that dwarfs are newcomers. In Section 5, we also show that stellar systems (GCs and dwarfs) with large eccentricity are actually affected by MW tides, and then

★ E-mail: francois.hammer@obspm.fr

© 2023 The Author(s)
Published by Oxford University Press on behalf of Royal Astronomical Society

Downloaded from https://academic.oup.com/mnras/article/519/4/5059/7000207 by guest on 23 April 2024

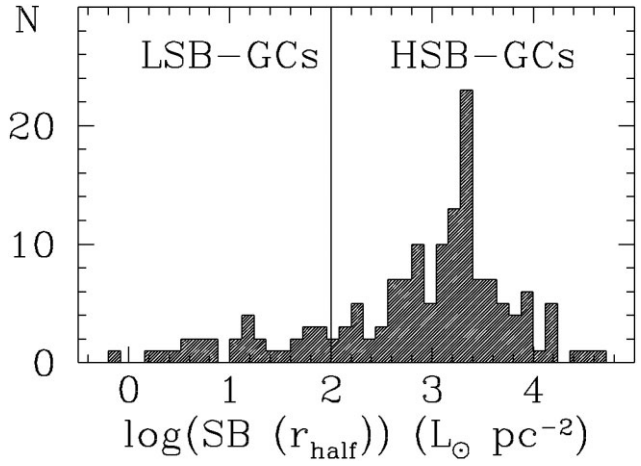

Figure 1. Distribution of globular cluster surface brightness in logarithmic scale. Surface-brightness in the *V*-band have been averaged within the half-light radius. The 127 HSB-GCs ($\log(\mathrm{SB/L_\odot\,pc^{-2}}) > 2$) distribute almost along a gaussian with a peak at $\log(\mathrm{SB/L_\odot\,pc^{-2}}) = 3.3$. The 29 LSB-GCs include the GCs represent the low-surface brightness tail of the GC distribution, and they are on average 315 times fainter than HSB-GCs.

how dwarfs have different nature depending on whether they belong to the Vast Polar structure or not.

2 DATA AND DERIVED ORBITAL PARAMETERS

The goal of this paper is to investigate whether the intrinsic properties of MW halo inhabitants are consistent with self-equilibrium or determined by their orbital properties. Despite the importance of previous theoretical investigations, few has been done on the observational side, and this paper aims at filling this gap.

Here we consider all stellar systems as a single class aiming not to distinguish between globular clusters and dwarfs. Our motivation is two-fold: first, these systems have a similar range in stellar mass, and second, as pointed out by Marchi-Lasch et al. (2019), there are similarities between structural properties of ultra faint dwarfs and low-surface brightness GCs. This leads us to distinguish three different populations, the high-surface brightness (HSB-GCs, with $\log(\mathrm{SB}/L_\odot\,\mathrm{pc^{-2}}) > 2$), the low-surface brightness (LSB-GCs, with $\log(\mathrm{SB}/L_\odot\,\mathrm{pc^{-2}}) < 2$) globular clusters (see Fig. 1), and the dwarfs for which the surface brightness (SB) is similar or smaller than that of LSB-GCs. The classification by surface brightness is possibly more restrictive than that of Marchi-Lasch et al. (2019) in selecting LSB-GCs. It is also much more accurate, because it comes from the work of Baumgardt, Sollima & Hilker (2020) who significantly improve the determination of absolute luminosity, providing corrections that can be as high as two magnitudes in *V*-band. To do so, they counted individual stars using HST photometry, selecting them from their proper motion, colour-magnitude diagram, and radial velocity.

In the following, we have used the data[1] for 156 GCs from Baumgardt (2017), Baumgardt & Hilker (2018), Baumgardt et al. (2020), Baumgardt & Vasiliev (2021), Sollima & Baumgardt (2017), and their proper motions from *Gaia* EDR3 (Vasiliev & Baumgardt 2021). Tables C1 and C2 in Appendix C display the resulting orbital parameters (velocities and orbital radii), and their error bars for a MW model following Eilers et al. (2019, see also more descriptions in Jiao et al. 2021). For dwarfs, we are using the data from *Gaia* EDR3 (Li et al. 2021) using the same MW model, and same prescriptions for deriving parameters. The Eilers et al. (2019) model of the MW rotation curve includes a bulge, a thick and a thin disc following Pouliasis, Matteo & Haywood (2017). The halo is represented by a NFW model (Navarro, Frenk & White 1996) that requires a cut-off radius fixed at $R_{\rm vir} = 189$ kpc to avoid infinite mass; this reduces the effect of the mass exterior to a given radius in the potential calculation by $+4\pi G\rho_0\ R_s^2/(1+R_{\rm vir}/R_s)$ after combining equations (2.28) and (2.64) of Binney & Tremaine (2008), where $\rho_0 = 0.0106\ \mathrm{M_\odot\,pc^{-3}}$ is the central density of the halo and $R_s = 14.8$ kpc is the halo scale radius.

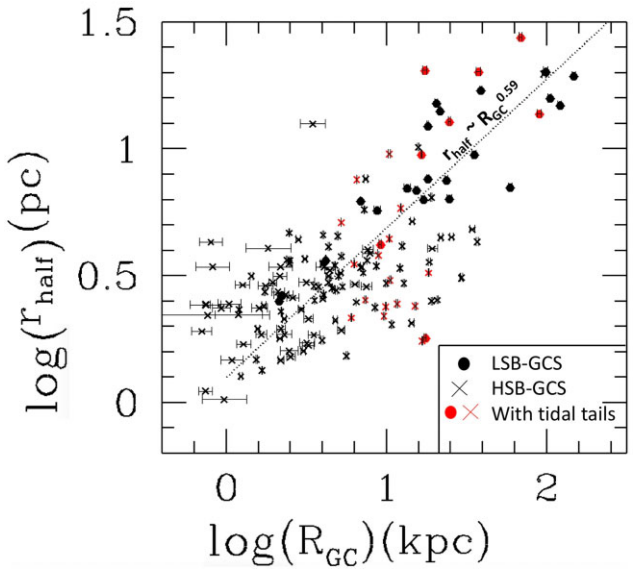

Figure 2. Half-light radius versus their galactocentric distances ($R_{\rm GC}$) for HSB-GCs (*crosses*) and LSB-GCs (*filled circles*). *Red symbols* identify GCs with tidal tails, which has been based on the compilation made by Zhang, Mackey & Da Costa 2022.

3 IS THERE A CORRELATION BETWEEN INTRINSIC AND ORBITAL PARAMETERS?

3.1 Correlation between half-light radius and pericentre

Pioneering studies of van den Bergh (1994), van den Bergh (2011), van den Bergh (2012) revealed the existence of a correlation between GC half-light radii and their galactocentric distances, $R_{\rm GC}$. Fig. 2 shows that it is still present despite significant progresses made in estimating GC distances, as well as their photometric parameters (Baumgardt 2017; Sollima & Baumgardt 2017; Baumgardt & Hilker 2018; Baumgardt et al. 2020; Baumgardt & Vasiliev 2021). For the 156 GCs listed in Table C1, it leads to a correlation[2] with $\rho = 0.63$, and the only difference with van den Bergh (2011) is that the slope of the relation is slightly less steep (0.59 instead of 0.66).

[1]Globular cluster data have been compiled by Holger Baumgardt, Antonio Sollima, Michael Hilker, Andrea Bellini & Eugene Vasiliev (see https://people.smp.uq.edu.au/HolgerBaumgardt/globular/).

[2]Along the manuscript we have used a Spearman's rank correlation ρ that does not assume any shape for the relationship between variables; the significance and associated probability of ρ have been tested using $t = \rho\sqrt{(n-2)/(1-\rho^2)}$, which is distributed approximately as Student's t distribution with $n-2$ degrees of freedom under the null hypothesis.

Downloaded from https://academic.oup.com/mnras/article/519/4/5059/7000207 by guest on 23 April 2024

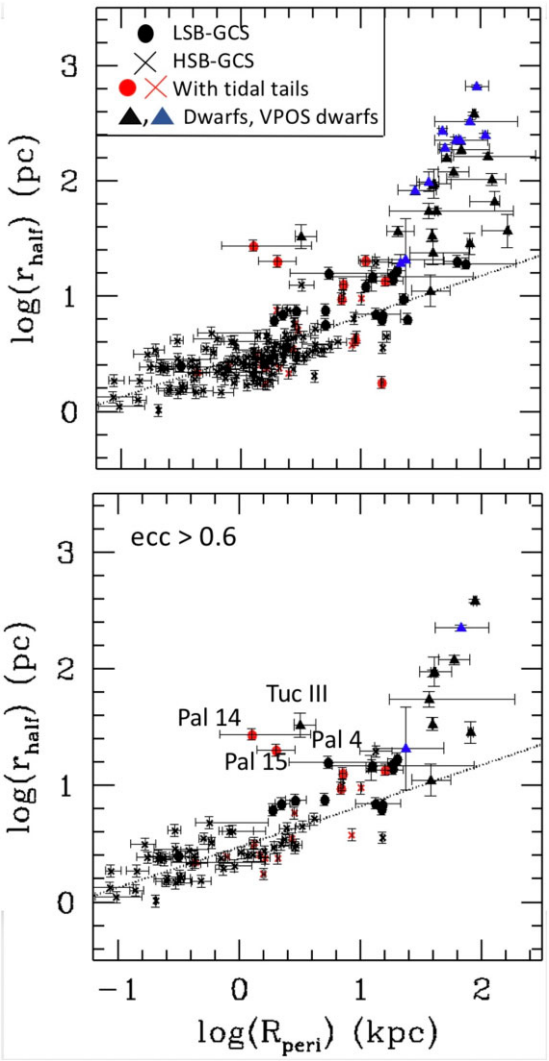

Figure 3. Half-light radius versus their orbital pericentre ($R_{\rm peri}$) for HSB-GCs (crosses), LSB-GCs (*filled circles*), and dwarf galaxies (*triangles*). The *dotted line* (slope = 0.33) indicates the correlation for the 156 GCs, which are shown in the *top panel* together with 30 dwarfs, while in the *bottom panel* only the 77 GCs and 12 dwarfs with orbital eccentricity larger than 0.6. Few stellar systems very offset from the correlation and suspected to be strongly tidally disrupted are labelled.

Such a correlation prompted van den Bergh (2011) to suggest that core-collapsed clusters have the tendency to be near the Galactic Centre. This is not unexpected from the theoretical side, since the inner GCs suffer stronger tidal forces from the MW. Within such a context, the most energetic GC stars may leave the system after gaining energy from tidal shocks, then lowering the system binding energy, finally leading to an adiabatic contraction when leaving the pericentre.

Since the half-light radius is a fundamental structural parameter, we investigate its dependency onto a pure orbital parameter specifically the pericentre, $R_{\rm peri}$. This has been firstly investigated on the basis of *Gaia* DR2 data by de Boer et al. (2019), but the error bars on pericentres were too large for providing robust conclusions. Using *Gaia* EDR3 data, we find a stronger correlation when replacing the galactocentric distance by the pericentre. Fig. 3 reveals that the half-light radius of 156 GCs correlates well with their orbital pericentres, with $r_{\rm half}$ following $R_{\rm peri}^{1/3}$ with $\rho = 0.70$, $t = 12$, with an extremely low probability that it occurs by chance, $P = 1.3 \times 10^{-23}$.

Few preliminary remarks can be made about the correlation shown in Fig. 3, which are particularly relevant when considering objects with different eccentricity, which we define as:

$$\mathrm{ecc} = \frac{R_{\rm apo} - R_{\rm peri}}{R_{\rm apo} + R_{\rm peri}}. \quad (1)$$

(i) The correlation becomes even more significant ($\rho = 0.79$ and $P = 9 \times 10^{-18}$) for half of the sample, i.e. the 77 GCs with high eccentricity (ecc > 0.6, see bottom panel of Fig. 3);

(ii) The above is true even after accounting for the few GCs that are fully off from the correlation, especially Pal 14, Pal 15, and Pal 4, and which are all with very eccentric orbits, while two of them possess tidal tails (see red dots);

(iii) Dwarf galaxies from Li et al. (2021) show a much steeper slope but with a less tight correlation ($\rho = 0.55$, $P = 2 \times 10^{-4}$ for 37 dwarfs).

The significant correlation shown in Fig. 3 suggests that MW tides could be at work, and that they are even more efficient for GCs with eccentric orbits. The strongest tidal shocks on GCs are generated as the cluster crosses the Galactic disc or passes through pericentre on a highly eccentric orbit (Binney & Tremaine 2008). However, one may wonder whether the observed correlation could be a hard-to-disentangle combination of star formation processes, and subsequent dynamical evolution in the hierarchical build-up of the Milky Way halo. Former studies have indicated how the MW may have filtered the different populations of stellar systems to establish the present-day GC population (Fall & Rees 1977, 1985; Gnedin & Ostriker 1997). In particular, Fall & Rees (1985, see their fig. 4) predicted that the combination of tides and thermal instabilities may lead to a decreasing density with the galactocentric distance, which seems quite consistent with the ($r_{\rm half}$, $R_{\rm GC}$) correlation shown in Fig. 2, and then with the ($r_{\rm half}$, $R_{\rm peri}$) correlation shown in Fig. 3.

A major drawback with this possibility is that the Fall & Rees (1985) scenario assumed a monolithic collapse for the initial formation of the MW. In the recent literature the favored formation scenario for spiral galaxies is through the hierarchical scenario, i.e. mostly through gas-rich major mergers (Hammer et al. 2005; Yang et al. 2008), which are essential in providing enough angular momentum into Galactic discs (Hammer et al. 2009; Hopkins et al. 2009, 2010; Stewart et al. 2009). This also applies to the MW, as evidenced by the finding of GSE imprints in the Energy-Angular momentum diagram (see Malhan et al. 2022 for imprints related to GCs Belokurov et al. 2018; Haywood et al. 2018). If GCs were formed initially as proposed by Fall & Rees (1977) and Fall & Rees (1985), their density-galactocentric distance relation would be rapidly diluted after one or more major merger.

3.2 Is the ($r_{\rm half}$, $R_{\rm peri}$) correlation due to MW tides?

Because $r_{\rm half}$ is much more correlated to $R_{\rm peri}$ than to $R_{\rm GC}$, one may conclude that (1) the correlation shown in Fig. 2 is generated by that in Fig. 3, and (2) it is a strong indication that GC structural parameters are impacted by pericentre passages. Simulations are necessary to go beyond that understanding, and we have used those made by Martinez-Medina et al. (2022), who tested how the GC half-light radii with different concentration parameter values can be affected by pericentre passages. Interestingly, they found that half-light radii of concentrated GCs have shrunk by ∼3 per cent after

Downloaded from https://academic.oup.com/mnras/article/519/4/5059/7000207 by guest on 23 April 2024

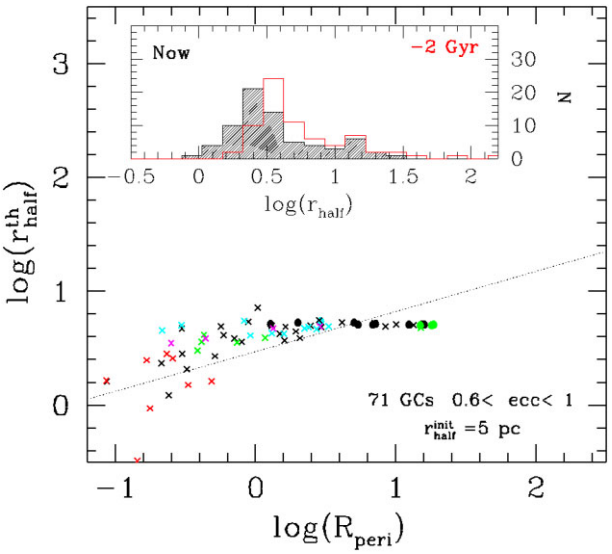

Figure 4. Predicted half-light radius (in parsec) versus orbital pericentre ($R_{\rm peri}$, in kpc) for HSB-GCs (*crosses*) and LSB-GCs (*filled circles*) after 2 Gyr evolution of GCs that were assumed having an initial half-light radius of 5 pc. The dotted line (slope = 0.33) indicates the correlation for the 156 GCs defined in Fig. 3. The *inset* shows the histograms of present-day GC $r_{\rm half}$ at present (*black*) and 2 Gyr ago (*red*).

one pericentre passage, while conversely, the least concentrated GCs show an expansion of their half-light radii by ∼7 per cent. In the following, we investigate a very simple model based on the Martinez-Medina et al. (2022)'s simulations, and accordingly to the latter, we have considered equal the impact of tidal shocks due to a point mass and to disc passages.

We have verified from the Harris (2010) compilation of 144 GCs that HSB-GCs have an average concentration parameter of $W_0 = 7.2$, which is quite similar to that of compact clusters chosen by Martinez-Medina et al. (2022, $W_0 = 8$). We have further assumed a linear interpolation of the half-light radius evolution with pericentric passage (see details in Appendix A), from $W_0 = 8$ GCs ($\Delta r_{\rm half}/r_{\rm half} = -3$ per cent) to $W_0 = 2$ GCs ($\Delta r_{\rm half}/r_{\rm half} = +7$ per cent). To test how tidal shocks may explain the ($r_{\rm half}$, $R_{\rm peri}$) correlation, we have adopted a single initial half-light radius for all GCs to verify how it evolves in Fig. 4. The latter shows that the correlation is mostly retrieved including its significance ($\rho = 0.76$) and its slope (0.39). It indicates that the modest loss of half-light radius at each pericentre is compensated by the numerous pericentre passages (up to 100 for a 2 Gyr duration) experienced by the closest GCs to the centre.

The evolution of GC half-light radii is also illustrated in the inset of Fig. 4. Assuming the present-day GC $r_{\rm half}$ and an evolution driven by tidal shocks, one finds that the peak of the distribution evolves to $r_{\rm half} = 2.5$ pc nowadays from 3.5 pc 2 Gyr ago. One may also notice that the correlation is better retrieved after considering eccentric GCs. When including the less eccentric GCs (ecc < 0.6), the correlation significance and the slope drop to 0.54 and 0.22, respectively. We have also tried larger look back times, such as e.g. 6 instead of 2 Gyr ago. It has led to larger slopes, which are due to extremely small theoretical GCs due to their extremely large number of pericentre passages. The above results show the limits of our exercise: the most eccentric GCs are expected to be the most affected in the last 2 Gyr, while extending our test to much larger elapsed periods leads to unrealistic values for $r_{\rm half}$ since the pericentre is likely evolving with time.

We also notice that the points with $\log(R_{\rm peri}) > 0.5$ in Fig. 4 do not follow the correlation, and that the corresponding GCs have essentially kept their initial $r_{\rm half}$ value. They are mostly LSB-GCs, and we find that they have experienced only a single pericentre passage during the 2 Gyr elapsed time, i.e. they have not yet been reshaped by tides. Given that actual LSB-GC (as well as dwarf) half-light radii are mostly above the $r_{\rm half} \sim R_{\rm peri}^{1/3}$ line in Fig. 3, this indicates that the their structural parameters are mostly fixed by their star formation processes, or alternatively by another mechanism (see section 5). Our model is surely over-simplified, and a more sophisticated model is necessary, though beyond the scope of the present paper. Such a more detailed study should account for the full evolution of GCs, including their orbital history, as well as for the MW mass evolution, and this would very useful for disentangling the different effects on half-mass radii from tides and from star formation. On the other hand, it is unlikely that the present-day distribution of GC half-light radii can be attributed to their initial distribution function, while accounting for existing simulations (Martinez-Medina et al. 2022) provides sufficient evidence that GCs are shaped by MW tides.

Figs 3 and 4 show that at present-day, eccentric GCs with small pericentres are the most impacted by tides. Appendix A details how the correlation between GC surface brightness and concentration parameter has been established. We have also determined that the few GCs (especially Pal 14, Pal 15, and Pal 4) that escape the correlation shown in Fig. 3 are heavily tidally stripped or shocked at present-time (see Appendix B).

4 CALIBRATING THE EPOCH OF GC EMERGENCES IN THE MW HALO

The correlation between an intrinsic quantity, the half-light radius, with an orbital parameter, the pericentre, is suggestive of the important role played by the MW potential in shaping GCs. However, to compare its impact on the various inhabitants of the halo, we need to calibrate their relative epochs of infall, or alternatively, the time when they have emerged into the MW halo. This can be approximated from numerical simulations (Boylan-Kolchin et al. 2013), which show that the total energy is decreasing with infall look-back time, similarly to the onion skin model initiated by Gott (1975) for explaining the outer density profile of elliptical galaxies. This does not come at a surprise, since the more orbits made by a stellar system in the halo, the more dissipated its energy would be,[3] e.g. by encountering other subsystems including giant molecular clouds, or at passages through the MW disc, or near the bulge.

We estimate the epochs of infall with the help of the identifications of substructures in the Galactic halo made by Malhan et al. (2022), which have been assumed to be linked to past merger events. By studying the associations of these events with GCs, Malhan et al. (2022) have been able to identify substructures associated to the bulge to the disc to a novel substructure called Pontus, and also to *Gaia* Sausage Enceladus (GSE), LMS1-Wukong, and Sgr. To this we have added the Kraken event identified by Kruijssen et al. (2020), because it could be the earliest merger that can be identified in the MW halo. We also notice that Kruijssen et al. (2020) associated to GSE some of the GCs associated to Pontus by Malhan et al. (2022).

[3]This also applies to angular momentum or to pericentre, both quantities that should decreases with time; however, small pericentre or angular momentum values can also be associated to radial orbits, and hence these two quantities cannot be taken as time proxy.

Downloaded from https://academic.oup.com/mnras/article/519/4/5059/7000207 by guest on 23 April 2024

Fig. 5 presents the relation between the total energy and the angular momentum for eccentric (bottom) and non-eccentric (top) stellar system. First, it is very similar to that between the total energy and the pericentre, simply because the angular momentum correlates extremely well with the pericentre. Second, the total energy appears to be well associated to the time occurrence of the merger events. In most halo substructures, GCs show a narrow range in energy suggesting that the total energy is a proxy of the infalling time.

If correct, it would assume a very early epoch for the bulge GCs as indicated by their ages (Kruijssen et al. 2019). This is indeed corroborated by the fact that most bulge GCs have their orbits circularized, as indicated by the comparison between the two panels of Fig. 5 showing that most bulge GCs have low-eccentricity orbits. We have followed Kruijssen et al. (2020) by indicating Kraken as being the most ancient detected merger in the MW halo, this followed by Pontus, and that by GSE with an approximated age of 8–10 Gyrs, and for which ages have been derived from that of their associated GCs (Kruijssen et al. 2019). The methodology of Kruijssen et al. (2020) is to compare the observed GC age distribution from Kruijssen et al. (2019) to that derived from cosmological simulations. They associate a merger with an epoch defined as 'as the moment at which SUBFIND can no longer find a bound subhalo, and the subhalo is therefore considered to have merged into the halo of the central halo'. In principle, this corresponds to the time when the merger is close to completion, though it appears quite uncertain since, in their subsequent work, Kruijssen et al. (2020) assumed instead that it corresponds to the entrance of the system into the halo. On the other hand, during merging encounters, star formation usually reaches its peak at the time of merger (see their fig. 4 Puech et al. 2012) rather than at first pericentre (Di Matteo et al. 2008). Such star formation at merging is likely accompanied with the formation of proto-GCs.

However, the above uncertainty has small consequences in the case of major merger events such as Kraken or GSE, because due to dynamical friction, the time between halo entrance and final merger is relatively small and similar to their quoted uncertainties, i.e. $\Delta T \sim$ 2 Gyr. The situation for Sgr is very different, because (1) the merger is far from being completed, and (2), it is likely a minor merger. The Sgr merger event has been considerably studied and modelled, since conversely to former merger events, the Sgr core, associated GCs, and stream are still easily recognizable.[4] It is likely that many Sgr GCs have taken their birth into the Sgr surrounding material, i.e. before its entrance into the MW halo. Because we are interested in the location of Sgr GCs into the ($E_{\rm tot}$, h) diagram, their total energy should be quite similar to that at the Sgr infall time, or its first entrance into the halo.

To estimate the Sgr infall time, we have used the most accurate analyses of the star formation history (SFH) of Sgr. We further assume that before entering the MW halo, the Sgr progenitor should have been considerably gas-rich as suggested by the distribution of gas-rich dwarfs in the Local Group (Grcevich & Putman 2009). One can then estimate its first infall and gas depletion times using the Sgr SFH. Sgr hosts populations of different ages as seen in deep HST photometry (Siegel et al. 2007) that clearly displays several turn-offs in their colour-magnitude diagrams. From the photometry and detailed abundances for a sample of giant stars within 9′ from the centre of M54, Mucciarelli et al. (2017) found a double-peaked metallicity distribution function, with peaks at −1.5 and −0.5. They also claimed that the chemical evolution of Sgr implies a strong gas loss occurring between 2.5 and 7.5 Gyr ago, which they presume occurring at the first passage at pericentre of Sgr following its infall into the Milky Way. More recently, Alfaro-Cuello et al. (2019) using deep, albeit low resolution, spectroscopic data that covers only the inner region of M 54 (2.′) radius, to be compared to 7.′4 of the tidal radius of the cluster) claimed the detection of three different populations a young one (2.3 Gyr old), an old population (12 Gyr old), and an intermediate-age population (4.3 Gyr old) that is more widespread. The young population can coincide with the last event of gas depletion that probably occurs in the very central Sgr region, while the intermediate-age population is suggestive of a longer event during which ram-pressure progressively removes the gas from Sgr, while star formation is sustained by gas pressurization from ∼6 to 3 Gyr ago (see fig. 7 of Alfaro-Cuello et al. 2019).

Using SDSS photometry and spectroscopy de Boer, Belokurov & Koposov (2015) found that the SFH of the Sgr Stream and found that the SFH increases 6 Gyr ago with a peak 5 Gyr ago and then a rapid decline 4 Gyr ago (see their fig. 6). Interestingly, the most recent models of Sgr (Vasiliev, Belokurov & Erkal 2021; Wang et al. 2022a) assumed an infall from 3 to 4.7 Gyr ago. Finally an infall more recent than 6 Gyr ago is necessary to account for the age of Whiting 1 (6.5 Gyr old). Putting all the available evidence together we conclude that the first infall of Sgr must have occurred between 4 and 6 Gyr ago.

Besides GCs, Fig. 5 also shows how other dwarfs than Sgr are distributed in the ($E_{\rm tot}$, h) plane (see also Hammer et al. 2021). Most of the dwarfs belonging to the Vast Polar Structure perpendicular to the disc (VPOS, see Pawlowski et al. 2014; Pawlowski 2018; Li et al. 2021) show small eccentricities and follow the line with $V_{\rm rad} = 0$ (or $V_{\rm 3D} = V_{\rm rot}$), i.e. a minimal energy for a given angular momentum (see blue triangles). This has been attributed by Hammer et al. (2021) to the fact that most of them are newcomers and have recently lost their gas due to ram-pressure, which affects more their radial velocities, leading to the observed anisotropic distribution of velocities (Cautun & Frenk 2017; Li et al. 2021). However, there are other dwarfs showing high-energy and high-orbital eccentricity, including dwarfs associated to the LMC on the basis of their relative *Gaia* motions (Erkal & Belokurov 2020; Patel et al. 2020). Because of that, we have considered two substructures of the VPOS, one still called the VPOS (blue triangles), the other called LMC for associated dwarfs to this galaxy (cyan triangles).[5] Dwarfs that are not in the VPOS are shown in Fig. 5 as black triangles, and many of them have significant radial velocities, as indicated by their offset from the $V_{\rm 3D} = V_{\rm rot}$ line.

5 DISCUSSION

5.1 Relating total energy to the epoch when stellar systems entered the MW halo

The estimated lookback times of entry into the MW halo of different populations of GCs of Kruijssen et al. (2019) can be compared to their orbital binding energies (see Fig. 5 and section 4). This is shown in Fig. 6, which has been built on the basis of the narrow total energy range shown by each identified structures in the MW halo.

[4] Besides M 54, Arp 2, Terzan 7, Terzan 8, Whiting 1, Pal 12 that are part of the Sgr system (Bellazzini et al. 2020), we have quoted Segue II, Willman I, and Tucana III as potential companions of Sgr, because their poles, energy, and angular momentum are either similar, or with an inverted angular momentum; for example, in the current potential used in this paper, Segue II appear to have encountered Sgr less than one hundred million years ago.

[5] It includes, Carina II, Carina III, and Phoenix II, all with positive energy for that MW mass model (not represented in Fig. 5), and also Horologium I, Hydrus I, and Reticulum II.

Downloaded from https://academic.oup.com/mnras/article/519/4/5059/7000207 by guest on 23 April 2024

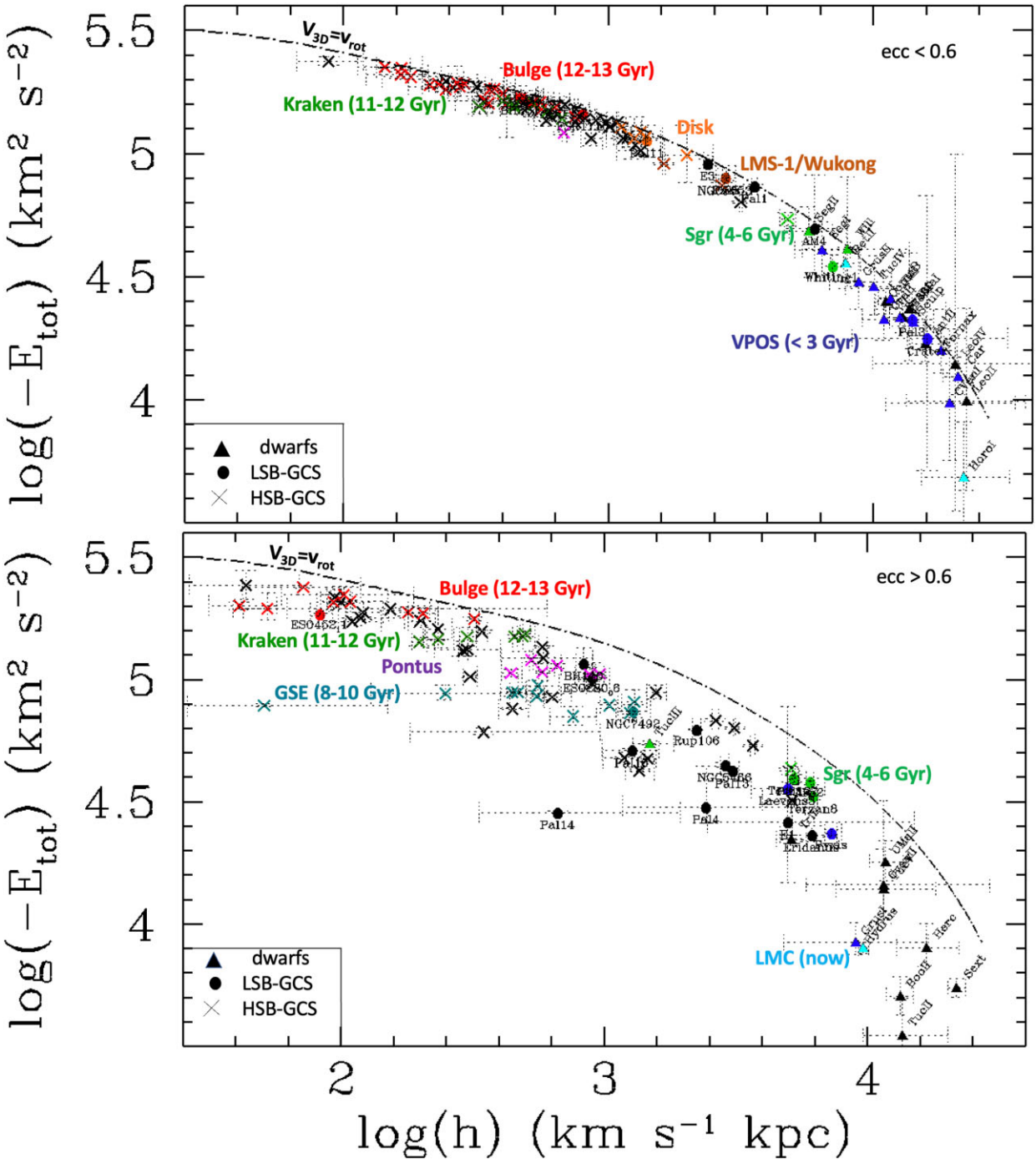

Figure 5. Total energy versus the angular momentum, $h = R_{GC} \times V_{tan}$ in logarithmic scale, for HSB-GCs (crosses), LSB-GCs (*filled circles*), and dwarfs (*triangles*). Identified structures by Malhan et al. 2022 and Kruijssen et al. 2020 are added by different colours indicated in the figure. VPOS dwarfs and GCs are also shown in *blue*, while the few dwarfs associated to the LMC are shown with *cyan*. The *top panel* shows 79 GCs and 20 dwarfs with eccentricities smaller than 0.6, while the *bottom panel* shows the 77 GCs and 15 dwarfs with eccentricities larger than 0.6. The *dotted line* shows the limit that cannot be passed by any orbits, as it is fixed for $V_{rad} = 0$ and a circular orbit (lowest possible energy for a given angular momentum). Note that few dwarfs having a positive energy are not represented, including Leo I in the VPOS, Carina II and III and Phoenix II, all related to the LMC, and Hydra II and Leo V.

Two simple mechanisms could explain such a relation for which stellar systems coming the earlier in the MW halo have smaller energy:

(i) The MW mass increase with time, which imposes a low energy for early-coming stellar systems;

(ii) Early-coming stellar systems have experienced several orbits, and then have large chances to encounter other systems to lose further their energy.

Fig. 5 shows the distribution of previous mergers in the MW, illustrating also that dwarfs possess higher total energy, and angular

Downloaded from https://academic.oup.com/mnras/article/519/4/5059/7000207 by guest on 23 April 2024

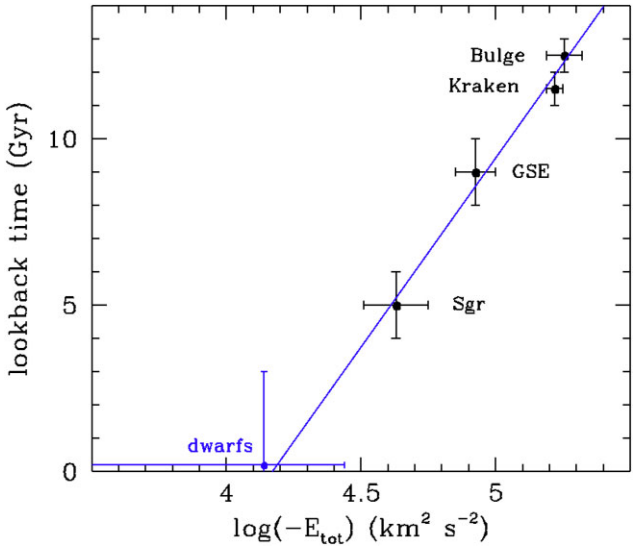

Figure 6. Lookback time of stellar system entry in the Milky Way halo as a function of current binding energy for different families of globular clusters, and for the 25 dwarf galaxies that do not belong to the low energetic Sgr system (excluding then Sgr, Segue II, Tucana III, and Willman I) or to the high-energetic LMC system (Carina II, Carina III, Horologium I, Hydrus I, Phoenix II, and Reticulum II). The *blue line* is a quick linear fit. A naïve interpretation is that dwarf satellites with $\log(-E_{\rm tot}/[{\rm km^2\,s^{-2}}]) < 4.17$ are on their initial approach, a value very close to the logarithm of the average energy (4.14) of 25 dwarfs (see text), whose scatter provides an upper limit of $-E_{\rm tot} = 4.34$. The latter combined with the linear fit suggests a lookback time of halo entry smaller than 3 Gyr.

momentum than Sgr and that of most GCs. The time elapsed between GSE and Sgr events is ∼4 Gyr, corresponding to a difference of energy of 0.25 dex (a factor ∼1.8). Extrapolating the same energy difference towards higher energies would lead to an energy value right at the average value for dwarfs as indicated in Fig. 6. Even if the total energy cannot be taken as a very precise clock, it suggests that most dwarfs are new or recent (<3 Gyr) comers into the MW halo (see also Hammer et al. 2021). Another clue for that is the very large scatter presented by dwarfs in the ($E_{\rm tot}$, h) plane. This is because newcomers may have different origins, and then possess different initial energies and angular momenta.

This contradicts several studies making the assumption that many dwarfs are long-lived satellites of the MW for nearly a Hubble time. Such an assumption neglects, e.g. the impact of the MW mass evolution. For example, in ΛCDM cosmology, the mass growth of the Milky Way since the epoch when bulge GCs were accreted ($z = 4.5$) is roughly a factor 50 (from fig. 5 of van den Bosch 2002). With such a small MW mass, only bulge GCs with the largest binding energies could be bound, while it is unlikely that low-binding energy dwarfs that lie at large distances can be captured at the same time.

5.2 The evolution of half-light radius with total energy and look-back time

The top panel of Fig. 7 shows how the half-light radius of the 156 GCs correlates with the total energy, i.e. smaller the energy, smaller the half-light radius. From the slope of the relation one finds that $r_{\rm half}$ follows $(-E_{\rm tot})^{-1.0}$, with a correlation of $\rho = -0.69$ associated to an extremely low probability that it occurs by chance, $P = 1.2 \times 10^{-23}$. This just indicates that bulge GCs (average $r_{\rm half} = 2.5$ pc) are smaller than GSE GCs (average $r_{\rm half} = 3.6$ pc), which are smaller than Sgr GCs (average $r_{\rm half} = 9.7$ pc). Since the total energy gives a proxy of the look-back time (see Figs 5 and 6), it implies that the half-light radius of GCs is decreasing with the time spent into the MW halo.

The correlation between half-light radius and total energy followed by the GCs is not similar for dwarfs, which are far much more scattered in the ($E_{\rm tot}$, $r_{\rm half}$) plane. In particular, many dwarfs (and all the classical dwarfs) lie well above the correlation. However, the bottom panel of Fig. 7 illustrates a different behaviour for GCs and dwarfs with eccentric orbits (ecc > 0.6). First, eccentric GCs show a more robust correlation between their half-light radii and their total energies (77 GCs, $\rho = -0.82$, $P = 1.7 \times 10^{-29}$) also with a slope of −1.0. Second, dwarfs appear to fall well within this correlation, thought with a larger scatter. It suggests that all eccentric stellar systems in the MW halo follow the same ($E_{\rm tot}$, $r_{\rm half}$) relation. The average half-light radii of eccentric GCs associated to the Bulge, to GSE, to Sgr, and to dwarfs are 1.95, 3.6, 9.8, and 83.5 pc, respectively, implying a decrease with the time elapsed into the halo. Such a decrease has been theoretically investigated for GCs (Aguilar et al. 1988; Gnedin & Ostriker 1999) since eccentric systems passing near their pericentres are likely affected by MW tidal shocks. This increases the internal energy of their stars, leading the least bound to be expelled. Then, after GCs have lost mass, they contract adiabatically when leaving the pericentre towards the apocentre.

This in turn enables the formation of tidal structures formed from stars tidally ejected from the cluster. This is well illustrated by the occurrence of tidal tails in GCs from Zhang et al. (2022, see their Table 3): only 9 per cent (7 among 79) of ecc < 0.6 GCs possess tidal tails, which contrasts with 22 per cent (17 among 77) of eccentric GCs (ecc > 0.6). Appendix B shows that three GCs (Pal 4, Pal 14, and Pal 15) are tidally disrupted since they have their tidal radii smaller than $r_{\rm half}$. Two of them possess strong tidal tails: Pal 14 (Sollima et al. 2011) and Pal 15 (Myeong et al. 2017). Despite the observational efforts (Ibata et al. 2021; Zhang et al. 2022), there is still a possibility that some tails have not been discovered yet, and we would like to suggest deep observations of Pal 4.

The most tidally disrupted GCs by the MW that are labelled in Fig. 3 are LSB-GCs. LSB-GC have sufficiently small densities to be strongly affected by MW tides, despite their large pericentres (average $R_{\rm peri}$: 13.8 kpc). The latter value is six times larger than that for HSB-GCs, but this is largely compensated by the 300 times lower densities of LSB-GC compared to HSB-GCs. LSB-GCs have been suspected by Marchi-Lasch et al. (2019) to be recent comers into the MW halo, and we confirm this (see Figs 5 and 7), simply because their average total energy ($E_{\rm tot} = -7.9 \times 10^4$ km^{2}s^{-2}) is significantly higher than that of HSB-GCs ($E_{\rm tot} = -15.7 \times 10^4$ km^{2}s^{-2}).

5.3 Dichotomy between eccentric and non-eccentric dwarfs

Almost all VPOS dwarfs have low eccentricity, while most other dwarfs (including the five LMC related dwarfs) have eccentric orbits. The latter are almost all ultra-faint dwarfs, except Sextans and Leo I.[6] Bottom panel of Fig. 7 shows that they follow the ($r_{\rm half}$, $E_{\rm tot}$) correlation made by eccentric GCs, which suggests that they could be affected by MW tides as well, as it was proposed by Hammer et al. (2019), Hammer et al. (2020). This is also supported by the tidally

[6]Leo I appears to be quite exceptional with respect to other classical dwarfs, first from its large distance, second from the fact that it would be the only unbound classical dwarf for our MW mass model;. this is also true after adopting PM values from the HST (Casetti-Dinescu et al. 2022) since they are very similar to those from *Gaia* EDR3.

Downloaded from https://academic.oup.com/mnras/article/519/4/5059/7000207 by guest on 23 April 2024

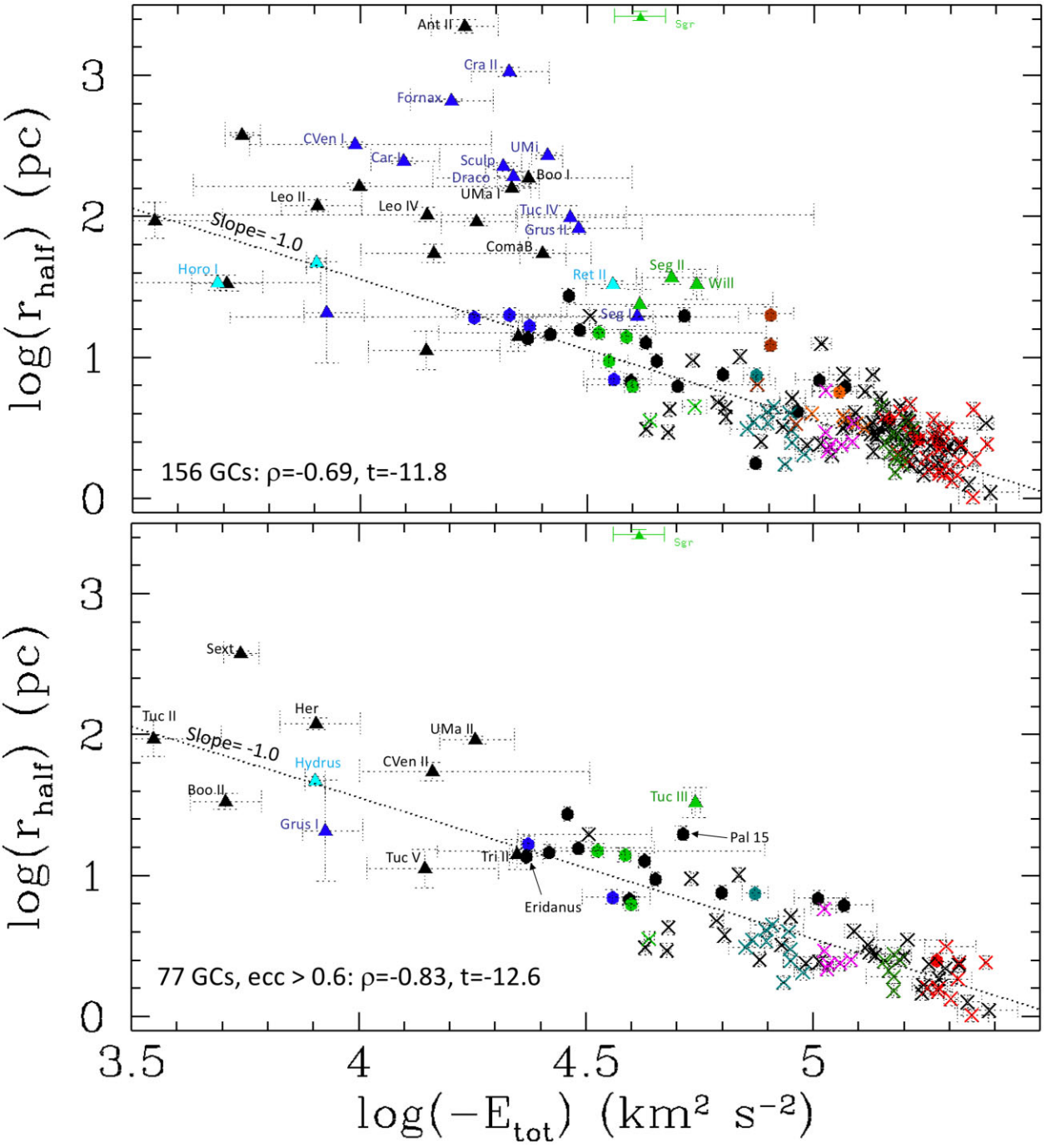

Figure 7. Total energy versus half-light radius in logarithmic scale, for HSB-GCs (crosses), LSB-GCs (full dots), and dwarfs (triangles). Identified structures by Malhan et al. 2022 and Kruijssen et al. 2020 are represented by the colour codes used in Fig. 5. VPOS dwarfs and GCs are also shown in blue colour, while the few dwarfs associated to the LMC are shown with cyan colour. The top panel shows 156 GCs and 35 dwarfs (those with ecc < 0.6 are labelled), while the bottom panel shows the 77 GCs and 15 (labelled) dwarfs with eccentricities larger than 0.6. The dotted line shows the fit of the GC points in the top panel, and of both GCs and dwarfs in the bottom panel, and the significance of the correlation is given on the bottom-left of each panel.

disrupted properties of Tucana III (Drlica-Wagner et al. 2015), and perhaps of Triangulum II (Martin et al. 2016). This may further apply to Hercules, which could be also tidally disrupted (Küpper et al. 2017; Garling et al. 2018). In the near future, we intend to verify whether all eccentric and energetic ultra-faint dwarfs have morphologies and kinematics consistent with being tidally disrupted.

The dichotomy between low-eccentric VPOS dwarfs and other dwarfs with high eccentricity, including those apparently linked to the LMC is also reflected in Fig. 5. VPOS dwarfs lie near the $V_{\rm rad} = 0$ line in Fig. 5, while almost all other dwarfs have still a significant radial velocity and lie much further from this line. It suggests that dwarfs could have been shaped by different combinations of tides and ram pressure effects:

(i) VPOS dwarfs with low eccentricities include almost all classical dwarfs (but Sextans and Leo I), and one may conjecture that it

Downloaded from https://academic.oup.com/mnras/article/519/4/5059/7000207 by guest on 23 April 2024

takes more time for ram-pressure to remove gas from more massive dwarfs; if correct, it means that ram pressure is particularly efficient to slow them down especially along their radial motion, explaining the observed velocity asymmetry for dwarfs (Cautun & Frenk 2017; Hammer et al. 2021), as it comes from especially from massive dwarfs of the VPOS;

(ii) Non-VPOS (and LMC-associated) dwarfs are mostly eccentric and ultra-faint dwarfs, and their gas could have been almost instantaneously removed by ram pressure, which would have preserve their orbit eccentric, while their half-light radii could be affected by both tides and ram pressure;

(iii) Because of their relatively recent infall, both VPOS and non-VPOS dwarfs may have lost their gas at relatively recent epochs (<3 Gyr), leading to an expansion of their residual stars due to a loss of gravity (Hammer et al. 2019, 2020). Such a mechanism could explain why their half-light radii is much larger than what is expected from the ($r_{\rm half}$, $R_{\rm peri}$) correlation in Fig. 3.

The above confirms that *Gaia* EDR3 results are sufficiently robust to avoid specific corrections to dwarf tangential velocities as proposed by Correa Magnus & Vasiliev (2022) and Pace, Erkal & Li (2022), even if this could be necessary for a few extremely faint dwarfs having proper motions with very large error bars.

5.4 Some lessons about the MW mass assembly

Fig. 5 provides useful informations about the origin of each merger having affected the MW. Pontus and GSE GCs are all with high eccentricity, while bulge and disc GCs are mostly made of systems with low eccentricities. This indicates that GSE and Pontus were likely related to a very eccentric infall of their progenitors. Part of the eccentricity of the GSE GC orbits may come from an orbit radialization (Vasiliev, Belokurov & Evans 2022), but this could apply only to the GSE progenitor, and not to the associated GCs, because Vasiliev et al. (2022) found that radialization is not efficient for very large mass ratios, i.e. GC masses are tiny in comparison to that of the MW or of its bulge. Interestingly, the eccentric GSE GCs appear to be more compact than expected from the relation shown in the top panel of Fig. 7, which is consistent with the fact that they are actively tidally shocked.

At increasing energies, one finds that the Sgr system eccentricity is in between that of bulge and GSE GCs while the Sgr eccentricity is 0.66. However, the situation of the Sgr dwarf appears to be rather exceptional: it is very offset from the ($r_{\rm half}$, $E_{\rm tot}$) correlation of the bottom panel in Fig. 7, while it possesses the most prominent system of tidal tails. Perhaps this is just due to the fact that despite its large eccentric orbit, the initial Sgr was so massive that it took more time for the MW to strip it efficiently, and have it joining the correlation of Fig. 7. The simulations by Wang et al. (2022b) show that after 1.5–2 Gyr from now, almost all the stars in the extended Sgr will be removed, letting only the nuclear GC NGC 6715 that lie on to the correlation. One can also wonder how a dwarf like Triangulum II can share the same location in the ($E_{\rm tot}$, $r_{\rm half}$) plane as Eridanus, while the luminosity of the latter is 40 times larger. The same applies to Tucana III and Pal 15, which both display tidal tails. If both type of stellar systems are recent comers, this just means that MW tides may have affected similarly systems with different masses, and indeed tidal theory shows little effect on host to satellite mass ratio.

6 CONCLUSIONS

This paper shows that an intrinsic structural parameter such as the half-light radius depends on orbital parameters such as pericentre, orbital eccentricity, angular momentum, and total orbital energy. Orbital parameters have been derived from *Gaia* EDR3 with an unprecedented accuracy for both GCs (this paper, Appendix C) and dwarfs (Li et al. 2021). It results that the intrinsic GC sizes tightly depend on the orbital parameters, the smaller they are, the smaller their pericentre, angular momentum, and orbital energy. We have shown that this is likely due to the impact of MW tidal shocks that progressively shrink GC half-light radii.

We have also used the archaeological studies of the former mergers that occurred into the MW (Kruijssen et al. 2020; Malhan et al. 2022). Here, we have been able to characterize the infall time of each event from its total orbital energy. We have shown that the latter can be used as a proxy of the epoch when stellar systems have emerged in the MW halo. This provides a relatively simple interpretation of the properties of MW halo inhabitants:

(i) Bulge, Kraken, GSE, and Sgr GCs are inhabitants of the MW halo since ∼12–13, 11–12, 8–10, and 4–6 Gyr ago, respectively;

(ii) Most dwarfs are newcomers into the MW halo less than 3 Gyr ago, which is confirmed by their large total energy and angular momentum, as well as by the large scatter of their distribution in most fundamental relations;

(iii) VPOS dwarfs that include the most massive ones have a different behaviour than other dwarfs in both ($E_{\rm tot}$, h) and ($r_{\rm half}$, $E_{\rm tot}$) planes; first they have a minimal energy for their angular momentum meaning small eccentricity orbits, and second, most of their half-light radii are larger than expectations from the strong correlation between $r_{\rm half}$ and $E_{\rm tot}$ established for GCs, all properties consistent with a recent lost of their gaseous content due to ram-pressure from the MW halo;

(iv) Many ultra-faint dwarfs unrelated to the VPOS or related to the LMC possess high-orbital energy, suggesting that they came very late in the MW halo. Since their orbits are highly eccentric, and that they share the same dependency between $r_{\rm half}$ and $E_{\rm tot}$ than eccentric GCs, they could be affected as well by strong tidal effects. Such a behaviour is not unexpected, because even if late arrivals do not favor strong tidal effects, this could be compensated by their very low surface or volume densities.

This paper is the first one to investigate in detail the relation between structural and orbital parameters of MW inhabitants since the pioneering work of van den Bergh (2011). It also consolidates all the work made by *Gaia* EDR3 in predicting robust proper motions and tangential velocities, including their error bars. This is true also for most dwarf galaxies, because otherwise we would have not observed the dichotomy presented by VPOS and non-VPOS dwarf properties.

The correlations shown in this paper are made using a MW mass model following Eilers et al. (2019), assuming a total mass of $8.2 \times 10^{11}\,{\rm M}_{\odot}$, which has been purposely made for reproducing the MW rotation curve with a NFW halo. An advantage of this choice is that all GCs and almost all dwarfs have negative total orbital energies. One may wonder whether the results depend on this choice. We have investigated the three other models of the MW made by Jiao et al. (2021) that cover the largest possible mass range (from 2.3 to $15 \times 10^{11}\,{\rm M}_{\odot}$) able to reproduce the MW rotation curve. Main results of this paper are unaffected, because they depend on the relative positions of the stellar systems along the total energy axis, the latter being a proxy of the infall time.

We conclude that the MW tides and ram-pressure appear to be quite preponderant in shaping the structure of the halo inhabitants, which opens the road for studying their morphologies and their kinematics, to verify whether these properties can be influenced as well by the host, our Galaxy. This work may help the understanding of GC and

Downloaded from https://academic.oup.com/mnras/article/519/4/5059/7000207 by guest on 23 April 2024

dwarf origins, as well as testing sophisticated physical models of MW GCs such as that of Reina-Campos et al. (2022). It would be interesting to verify whether they could reproduce the ($r_{\rm half}$ and $R_{\rm peri}$) correlation found in Fig. 3. In principle, if accounting for tidal and ram-pressure effects due to the MW, the intrinsic dynamical evolution of the stellar systems can be traced back with a good accuracy in time, based on their present-day orbital energy.

ACKNOWLEDGEMENTS

We are very grateful to Frederic Arenou and Carine Babusiaux for their advices, namely to use *Gaia* EDR3 data and their statistics. We warmly thank Holger Baumgardt for his help in using his remarkable work in gathering, and producing very advanced data for globular clusters. We thank the referee for the very useful remarks that have substantially improved the manuscript. We are grateful for the support of the International Research Program Tianguan, which is an agreement between the Centre National de la Recherche Scientifique (CNRS) in France, Nathional Astronomical Observatories of China (NAOC), Institute of High Energy and Particles (IHEP), and the Yunnan University in China. Marcel S. Pawlowski acknowledges funding of a Leibniz-Junior Research Group (project number J94/2020) and a KT Boost Fund by the German Scholars Organization and Klaus Tschira Stiftung.

DATA AVAILABILITY

All necessary data used in this paper are available in the Tables of the Appendix C and in Li et al. (2021).

REFERENCES

Aguilar L., Hut P., Ostriker J. P., 1988, ApJ, 335, 720
Alfaro-Cuello M. et al., 2019, ApJ, 886, 57
Baumgardt H., 2017, MNRAS, 464, 2174
Baumgardt H., Hilker M., 2018, MNRAS, 478, 1520
Baumgardt H., Vasiliev E., 2021, MNRAS, 505, 5957
Baumgardt H., Sollima A., Hilker M., 2020, PASA, 37, e046
Bellazzini M., Ibata R., Malhan K., Martin N., Famaey B., Thomas G., 2020, A&A, 636, A107
Belokurov V., Erkal D., Evans N. W., Koposov S. E., Deason A. J., 2018, MNRAS, 478, 611
Bertin G., Varri A. L., 2008, ApJ, 689, 1005
Binney J., Tremaine S., 2008, Galactic Dynamics, 2nd edn. Princeton Univ. Press, Princeton
Boylan-Kolchin M., Bullock J. S., Sohn S. T., Besla G., van der Marel R. P., 2013, ApJ, 768, 140
Casetti-Dinescu D. I., Hansen C. K., Girard T. M., Kozhurina-Platais V., Platais I., Horch E. P., 2021, AJ, 163, 1
Cautun M., Frenk C. S., 2017, MNRAS, 468, L41
Correa Magnus L., Vasiliev E., 2022, MNRAS, 511, 2610
de Boer T. J. L., Belokurov V., Koposov S., 2015, MNRAS, 451, 3489
de Boer T. J. L., Gieles M., Balbinot E., Hénault-Brunet V., Sollima A., Watkins L. L., Claydon I., 2019, MNRAS, 485, 4906
Di Matteo P., Bournaud F., Martig M., Combes F., Melchior A. L., Semelin B., 2008, A&A, 492, 31
Drlica-Wagner A. et al., 2015, ApJ, 813, 109
Eilers A.-C., Hogg D. W., Rix H.-W., Ness M. K., 2019, ApJ, 871, 120
Erkal D., Belokurov V. A., 2020, MNRAS, 495, 2554
Fall S. M., Rees M. J., 1977, MNRAS, 181, 37P
Fall S. M., Rees M. J., 1985, ApJ, 298, 18
Garling C. et al., 2018, ApJ, 852, 44
Gnedin O. Y., Ostriker J. P., 1997, ApJ, 474, 223
Gnedin O. Y., Ostriker J. P., 1999, ApJ, 513, 626
Gott J., Richard I., 1975, ApJ, 201, 296
Grcevich J., Putman M. E., 2009, ApJ, 696, 385
Hammer F., Flores H., Elbaz D., Zheng X. Z., Liang Y. C., Cesarsky C., 2005, A&A, 430, 115
Hammer F., Flores H., Puech M., Yang Y. B., Athanassoula E., Rodrigues M., Delgado R., 2009, A&A, 507, 1313
Hammer F., Yang Y., Wang J., Arenou F., Puech M., Flores H., Babusiaux C., 2019, ApJ, 883, 171
Hammer F., Yang Y., Arenou F., Wang J., Li H., Bonifacio P., Babusiaux C., 2020, ApJ, 892, 3
Hammer F., Wang J., Pawlowski M. S., Yang Y., Bonifacio P., Li H., Babusiaux C., Arenou F., 2021, ApJ, 922, 93
Harris W. E., 2010, preprint (arXiv:1012.3224)
Haywood M., Di Matteo P., Lehnert M. D., Snaith O., Khoperskov S., Gómez A., 2018, ApJ, 863, 113
Hopkins P. F., Cox T. J., Younger J. D., Hernquist L., 2009, ApJ, 691, 1168
Hopkins P. F. et al., 2010, ApJ, 715, 202
Ibata R. et al., 2021, ApJ, 914, 123
Innanen K. A., Harris W. E., Webbink R. F., 1983, AJ, 88, 338
Jiao Y., Hammer F., Wang J. L., Yang Y. B., 2021, A&A, 654, A25
King I., 1962, AJ, 67, 471
Kruijssen J. M. D., Pfeffer J. L., Reina-Campos M., Crain R. A., Bastian N., 2019, MNRAS, 486, 3180
Kruijssen J. M. D. et al., 2020, MNRAS, 498, 2472
Küpper A. H. W., Johnston K. V., Mieske S., Collins M. L. M., Tollerud E. J., 2017, ApJ, 834, 112
Li H., Hammer F., Babusiaux C., Pawlowski M. S., Yang Y., Arenou F., Du C., Wang J., 2021, ApJ, 916, 8
Malhan K. et al., 2022, ApJ, 926, 107
Mamon G. A., 2000, in Combes F., Mamon G. A., Charmand aris V., eds, ASP Conf. Ser. Vol. 197, Dynamics of Galaxies: From the Early Universe to the Present. Astron. Soc. Pac., San Francisco, p. 377
Marchi-Lasch S. et al., 2019, ApJ, 874, 29
Martin N. F. et al., 2016, ApJ, 818, 40
Martinez-Medina L. A., Gieles M., Gnedin O. Y., Li H., 2022, MNRAS, 516, 1237
Massari D., Koppelman H. H., Helmi A., 2019, A&A, 630, L4
Mucciarelli A., Bellazzini M., Ibata R., Romano D., Chapman S. C., Monaco L., 2017, A&A, 605, A46
Myeong G. C., Jerjen H., Mackey D., Da Costa G. S., 2017, ApJ, 840, L25
Navarro J. F., Frenk C. S., White S. D. M., 1996, ApJ, 462, 563
Pace A. B., Erkal D., Li T. S., 2022, ApJ, 940, 136
Patel E. et al., 2020, ApJ, 893, 121
Pawlowski M. S., 2018, Mod. Phys. Lett. A, 33, 1830004
Pawlowski M. S. et al., 2014, MNRAS, 442, 2362
Pouliasis E., Matteo P. D., Haywood M., 2017, A&A, 598, A66
Puech M., Hammer F., Hopkins P. F., Athanassoula E., Flores H., Rodrigues M., Wang J. L., Yang Y. B., 2012, ApJ, 753, 128
Reina-Campos M., Keller B. W., Kruijssen J. M. D., Gensior J., Trujillo-Gomez S., Jeffreson S. M. R., Pfeffer J. L., Sills A., 2022, MNRAS, 517, 3144
Siegel M. H. et al., 2007, ApJ, 667, L57
Sollima A., Baumgardt H., 2017, MNRAS, 471, 3668
Sollima A., Martínez-Delgado D., Valls-Gabaud D., Peñarrubia J., 2011, ApJ, 726, 47
Stewart K. R., Bullock J. S., Wechsler R. H., Maller A. H., 2009, ApJ, 702, 307
Tollet É., Cattaneo A., Mamon G. A., Moutard T., van den Bosch F. C., 2017, MNRAS, 471, 4170
van den Bergh S., 1994, AJ, 108, 2145
van den Bergh S., 2011, PASP, 123, 1044
van den Bergh S., 2012, ApJ, 746, 189
van den Bosch F. C., 2002, MNRAS, 331, 98
Vasiliev E., Baumgardt H., 2021, MNRAS, 505, 5978
Vasiliev E., Belokurov V., Erkal D., 2021, MNRAS, 501, 2279
Vasiliev E., Belokurov V., Evans N. W., 2022, ApJ, 926, 203

Downloaded from https://academic.oup.com/mnras/article/519/4/5059/7000207 by guest on 23 April 2024

Wang H.-F., Yang Y.-B., Hammer F., Wang J.-L., 2022a, preprint (arXiv:2204.08542)
Wang H.-F., Hammer F., Yang Y.-B., Wang J.-L., 2022b, ApJ, 940, L3
Yang Y. et al., 2008, A&A, 477, 789
Yang Y., Hammer F., Fouquet S., Flores H., Puech M., Pawlowski M. S., Kroupa P., 2014, MNRAS, 442, 2419
Zhang S., Mackey D., Da Costa G. S., 2022, MNRAS, 513, 3136

APPENDIX A: RELATING CONCENTRATION PARAMETER AND SURFACE BRIGHTNESS

A considerable effort has been done by Baumgardt et al. (2020), who significantly improved the determination of absolute luminosity, providing corrections that can be as high as two magnitudes in *V*-band, especially for GCs affected by extinction. This implies that the surface brightness calculated by Baumgardt et al. (2020) is the best indicator, currently available, of the GC compactness, and does not depend on extinction effects. Fig. A1 allows to convert surface brightness into central concentration parameter W_0, after accounting for the correlation between the King compactness c and log (SB) ($\rho = 0.62$ for 70 GCs from Harris 2010 with eccentricity larger than 0.6). It results that we can approximate:

$$W_0 = 4.412 \times c, \tag{A1}$$

and

$$c = 0.291 \times \log(\mathrm{SB}) + 0.545, \tag{A2}$$

which leads to:

$$W_0 = 1.2834 \times \log(\mathrm{SB}) + 2.406. \tag{A3}$$

In the following, we adopt equation (A3) for attributing compactness to each individual GCs, and furthermore assumes that each cluster with $W_0 \geq 8$ (≤ 2) would have its half-light radius shrunk (expanded) by 3 per cent (by 7 per cent) at each pericentre passage (see, e.g. Martinez-Medina et al. 2022). Furthermore, we have interpolated the tidal shock effects on GCs for cluster having W_0 values from 2 to 8 adopting:

$$\Delta r_{\mathrm{half}}/r_{\mathrm{half}} = 0.015 \times (6 - W_0). \tag{A4}$$

Fig. 4 illustrates how eccentric GCs are affected by tides, following the scheme from Martinez-Medina et al. (2022), and deriving the number of pericentre passages from the orbital parameters given in Appendix C.

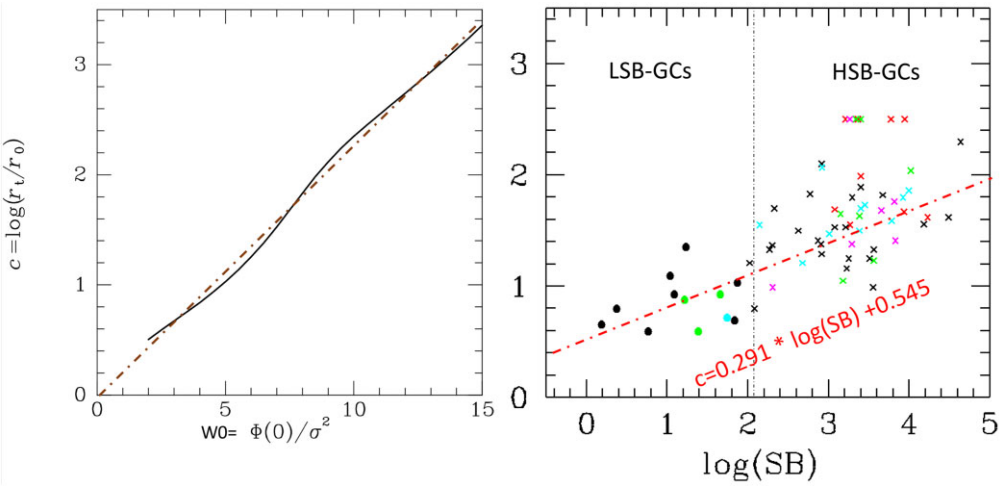

Figure A1. The left-hand panel shows the relationship between King profile compactness c and central concentration parameter W_0 based on fig. 4.9 of Binney & Tremaine (2008). The right-hand panel shows the correlation between the logarithm of the averaged surface brightness inside r_{half} and the King profile compactness c.

Downloaded from https://academic.oup.com/mnras/article/519/4/5059/7000207 by guest on 23 April 2024

APPENDIX B: TIDAL RADIUS AND SEARCH FOR GCS PRESENTLY DOMINATED BY TIDAL EFFECTS

We introduce the tidal radius, $r_{\rm tidal}$, and for quasi circular orbits, we adopt the definition from Innanen, Harris & Webbink (1983):

$$r_{\rm tidal} = \frac{2R_{\rm peri}}{3}\left[\frac{m_{\rm GC}}{M_{\rm MW}(R_{\rm peri})}\right]^{1/3}[1-\ln(1-{\rm ecc})]^{1/3}, \quad \text{(B1)}$$

in which the last term accounts for the effects related to eccentricity,[7] which we will call later, $\lambda = [1-\ln(1-{\rm ecc})]^{1/3}$. This term is introduced to compare an eccentric orbit with a circular one with the same total energy. Equation (B1) further assumes that the MW cumulative mass increases following the radius ($M_{\rm MW}(R_{\rm peri}) \sim R_{\rm peri}$). Such a condition is certainly fulfilled for radii <20 kpc, as shown by Jiao et al. (2021) from their analysis of the MW rotation curve.

After converting mass into density ($\rho(r)$) and radius (r) for both GC and the MW:

$$m_{\rm GC} = 2\,\frac{4}{3}\pi\rho_{\rm GC}(r_{\rm half})\,r_{\rm half}^3, \quad \text{(B2)}$$

$$M_{\rm MW}(R_{\rm peri}) = \frac{4}{3}\pi\rho_{\rm MW}(R_{\rm peri})\,R_{\rm peri}^3. \quad \text{(B3)}$$

Equation (B1) is equivalent to

$$r_{\rm tidal} \simeq 0.84\,r_{\rm half}\left[\frac{\rho_{GC}(r_{\rm half})}{\rho_{\rm MW}(R_{\rm peri})}\right]^{1/3}\lambda, \quad \text{(B4)}$$

where $\rho_{GC}(r_{\rm half})$ and $\rho_{\rm MW}(R_{\rm peri})$ are the mean mass densities of the GC inside its half-light radius, and of the MW inside $R_{\rm peri}$, respectively. Equation (B4) recovers the well-known fact that the tidal radius is that where the mean density matches that of the perturber (the MW) at that position. If $\rho_{GC}(r_{\rm half}) = \rho_{\rm MW}(R_{\rm peri})$, equation (B4) recovers the fact that the tidal radius matches precisely the half-mass radius for a GC median eccentricity of 0.6. In such a case, GCs can be considered as being dominated by MW tides.

However, the tidal formula of Innanen et al. (1983), as those of King (1962) and Bertin & Varri 2008, add a centrifugal term, which is only meaningful if the GCs where phase locked with the Milky Way (they are insufficiently rigid to be phase locked). Furthermore, their formulae are only relevant for quasi-circular orbits, where the tidal effects are long-lived. For eccentric orbits, the instantaneous tide is short lived and changes direction, and one should instead treat the tide as a shock and orbit average it. Following Mamon (2000) and its refinement by Tollet et al. (2017), a star of a MW satellite should suffer a velocity impulse equal to the tidal acceleration at pericentre times the duration $R_{\rm peri}/V_{\rm peri}$ of the pericentric passage. Mamon (2000) showed that eccentric orbits suffer tides that limit the system to a radius, where the mean density is not the mean density of the host at pericentre, but lower by roughly the square of the ratio of pericentric to circular velocity at pericentre. Therefore at fixed pericentre, the more eccentric orbits (with higher pericentric velocities) suffer less from tides. This is contrary to the instantaneous formulae of King (1962), Innanen et al. (1983), and Bertin & Varri (2008), which predict, at given pericentre, a too small tidal radius for eccentric orbits, and are thus only applicable for quasi-circular orbits and not for eccentric orbits.

The few GCs (especially Pal 14, Pal 15, and Pal 4) that escape the correlation shown in Fig. 3 have average density inside $r_{\rm half}$ close to that of the MW at their pericentres, even after accounting for the corrective factor introduced by Mamon (2000). It may indicate that low-density GCs on high-eccentric GCs are actively shaped by the MW tides, which perturb them sufficiently to move them off the correlation between ($r_{\rm half}$, $R_{\rm peri}$) shown in Fig. 3.

Because for all GCs, the half-light radius decreases with the pericentre following a tight 1/3 power law relation, it further suggests that for all GCs, their radii could have been settled by MW tides.

[7]Note that the eccentricity of Equation (B1) differs from the definition that we adopted in Equation (1).

APPENDIX C: ORBITAL PARAMETERS OF 156 GCS

Description of the Table C1 content: Column 1 lists the globular cluster name; Column 2–4 is the galactocentric distance, angle with respect to the North Galactic Pole and azimuthal angle; Column 5–7 gives the velocities in three dimensions; Column 8 provides the galactocentric tangential velocity, and Column 9 lists the total velocity in the Galactic rest frame.

Description of the Table C2 content: Column 1 lists the globular cluster name; Column 2 and 3 give the pericentre and the apocentre of the orbit; Column 4 is the eccentricity of the orbit; in Column 5, we provide the probability of the object being unbound. Column 6 gives the orbital phase.

Downloaded from https://academic.oup.com/mnras/article/519/4/5059/7000207 by guest on 23 April 2024

Table C1. Kinematic properties of globular clusters in galactocentric spherical coordinate system.

name	$R_{\rm GC}$ (kpc)	θ (deg)	ϕ (deg)	$V_{\rm r}$ (km s^{-1})	V_θ (km s^{-1})	V_ϕ (km s^{-1})	$V_{\rm tan}$ (km s^{-1})	$V_{\rm 3D}$ (km s^{-1})
AM 4	$24.6^{+0.7}_{-0.7}$	$49.3^{+0.2}_{-0.2}$	$124.2^{+0.5}_{-0.5}$	$-10.7^{+15.2}_{-16.4}$	$221.6^{+51.1}_{-46.9}$	$92.2^{+50.7}_{-48.9}$	$242.8^{+58.9}_{-55.7}$	$243.0^{+60.1}_{-55.8}$
Arp 2	$21.5^{+0.3}_{-0.3}$	$118.3^{+0.1}_{-0.1}$	$192.2^{+0.1}_{-0.0}$	$124.3^{+0.5}_{-0.5}$	$-269.3^{+4.7}_{-4.6}$	$-77.2^{+4.2}_{-4.6}$	$280.1^{+5.3}_{-4.9}$	$306.5^{+4.6}_{-4.3}$
BH 140	$6.8^{+0.0}_{-0.0}$	$92.8^{+0.2}_{-0.1}$	$36.3^{+2.2}_{-2.0}$	$192.3^{+13.8}_{-12.8}$	$-41.0^{+2.6}_{-3.0}$	$-114.0^{+7.3}_{-8.8}$	$121.1^{+9.4}_{-7.7}$	$227.2^{+16.8}_{-14.8}$
BH 176	$12.7^{+0.9}_{-0.8}$	$83.4^{+0.1}_{-0.1}$	$128.7^{+1.4}_{-1.5}$	$-34.9^{+10.1}_{-8.7}$	$-3.8^{+2.1}_{-2.0}$	$-267.0^{+19.8}_{-22.4}$	$267.0^{+22.4}_{-19.7}$	$269.4^{+23.2}_{-19.5}$
BH 184	$4.3^{+0.0}_{-0.0}$	$94.8^{+0.1}_{-0.1}$	$71.5^{+2.1}_{-2.1}$	$57.9^{+1.8}_{-1.8}$	$84.1^{+2.1}_{-1.9}$	$-116.6^{+3.2}_{-3.7}$	$143.9^{+4.0}_{-3.7}$	$155.1^{+4.3}_{-4.1}$
BH 229	$1.2^{+0.1}_{-0.1}$	$76.6^{+1.6}_{-1.8}$	$15.3^{+2.2}_{-1.9}$	$-103.2^{+5.8}_{-6.7}$	$226.5^{+2.4}_{-2.8}$	$8.7^{+6.2}_{-6.4}$	$226.7^{+2.7}_{-2.9}$	$249.1^{+5.1}_{-5.2}$
BH 261	$2.1^{+0.2}_{-0.2}$	$104.8^{+2.1}_{-1.8}$	$349.9^{+1.3}_{-1.5}$	$110.5^{+18.4}_{-18.9}$	$103.7^{+5.1}_{-4.9}$	$-182.2^{+6.2}_{-5.5}$	$209.9^{+6.9}_{-7.9}$	$237.2^{+2.7}_{-2.0}$
Crater	$146.9^{+3.1}_{-3.0}$	$42.0^{+0.0}_{-0.0}$	$90.1^{+0.1}_{-0.1}$	$-7.5^{+2.9}_{-3.9}$	$-81.9^{+63.4}_{-66.3}$	$13.0^{+75.1}_{-50.9}$	$107.9^{+72.4}_{-67.1}$	$108.1^{+72.2}_{-66.7}$
Djorg 1	$1.2^{+1.0}_{-0.4}$	$107.5^{+7.2}_{-6.6}$	$153.1^{+11.1}_{-14.7}$	$-250.9^{+78.4}_{-49.5}$	$65.9^{+8.7}_{-16.4}$	$-314.8^{+14.0}_{-34.1}$	$321.5^{+34.8}_{-14.9}$	$406.7^{+23.4}_{-10.0}$
Djorg 2	$0.8^{+0.1}_{-0.2}$	$116.9^{+8.8}_{-4.0}$	$216.7^{+21.5}_{-6.9}$	$7.5^{+72.1}_{-27.4}$	$75.8^{+11.4}_{-49.1}$	$192.4^{+3.7}_{-8.0}$	$206.6^{+2.7}_{-12.1}$	$209.0^{+1.5}_{-1.7}$
E 1	$120.2^{+2.4}_{-2.3}$	$137.7^{+0.0}_{-0.0}$	$72.7^{+0.1}_{-0.1}$	$-45.0^{+10.6}_{-10.2}$	$-5.4^{+32.8}_{-52.7}$	$7.5^{+33.9}_{-24.7}$	$41.1^{+44.3}_{-27.9}$	$63.0^{+34.4}_{-17.7}$
E 3	$9.1^{+0.1}_{-0.1}$	$106.3^{+0.3}_{-0.3}$	$52.6^{+1.3}_{-1.3}$	$25.6^{+1.0}_{-1.1}$	$-109.0^{+3.8}_{-3.7}$	$-234.5^{+4.4}_{-4.7}$	$258.7^{+5.6}_{-5.7}$	$259.9^{+5.7}_{-5.7}$
ESO 280-06	$13.5^{+0.6}_{-0.5}$	$109.7^{+0.3}_{-0.3}$	$158.5^{+0.4}_{-0.4}$	$61.0^{+1.0}_{-1.0}$	$55.5^{+3.8}_{-3.6}$	$-36.3^{+8.4}_{-8.9}$	$66.4^{+7.5}_{-6.4}$	$90.2^{+6.4}_{-5.4}$
ESO 452-11	$2.1^{+0.1}_{-0.0}$	$43.1^{+3.0}_{-3.2}$	$43.7^{+6.9}_{-5.2}$	$-94.5^{+2.4}_{-2.0}$	$37.4^{+1.4}_{-1.2}$	$-10.8^{+8.0}_{-7.4}$	$38.9^{+3.7}_{-2.3}$	$102.2^{+1.1}_{-0.9}$
ESO 93-8	$12.8^{+0.5}_{-0.5}$	$94.2^{+0.0}_{-0.0}$	$77.9^{+1.5}_{-1.6}$	$-4.1^{+6.2}_{-6.7}$	$6.1^{+1.4}_{-1.5}$	$-218.1^{+12.2}_{-11.7}$	$218.2^{+11.8}_{-12.1}$	$218.3^{+11.6}_{-12.3}$
Eridanus	$89.7^{+2.1}_{-2.1}$	$128.5^{+0.1}_{-0.1}$	$34.0^{+0.1}_{-0.1}$	$-141.5^{+1.3}_{-1.1}$	$-65.7^{+16.2}_{-16.0}$	$-8.9^{+12.1}_{-13.8}$	$67.9^{+15.6}_{-16.4}$	$156.7^{+6.7}_{-5.3}$
FSR 1716	$4.1^{+0.0}_{-0.0}$	$92.5^{+0.1}_{-0.1}$	$65.6^{+3.5}_{-3.6}$	$101.5^{+1.8}_{-2.2}$	$111.8^{+4.4}_{-4.2}$	$-157.0^{+6.9}_{-7.8}$	$192.7^{+8.9}_{-7.9}$	$217.7^{+8.8}_{-7.9}$
FSR 1735	$3.2^{+0.2}_{-0.2}$	$94.7^{+0.0}_{-0.1}$	$94.3^{+7.2}_{-9.5}$	$-121.6^{+8.8}_{-5.3}$	$-103.7^{+5.6}_{-5.1}$	$-104.8^{+12.3}_{-16.4}$	$147.8^{+8.4}_{-5.1}$	$191.9^{+3.0}_{-3.3}$
FSR 1758	$3.2^{+0.8}_{-0.8}$	$100.6^{+2.1}_{-1.4}$	$140.5^{+6.3}_{-10.6}$	$15.8^{+36.9}_{-63.4}$	$-193.0^{+28.9}_{-21.2}$	$328.6^{+2.6}_{-4.9}$	$382.2^{+7.0}_{-12.6}$	$382.5^{+10.2}_{-10.1}$
IC 1257	$19.2^{+1.1}_{-1.6}$	$68.8^{+0.3}_{-0.5}$	$204.0^{+0.7}_{-0.4}$	$-59.8^{+2.4}_{-2.1}$	$-4.8^{+3.3}_{-3.7}$	$9.8^{+15.6}_{-9.9}$	$12.9^{+13.3}_{-7.5}$	$62.1^{+2.3}_{-1.9}$
IC 4499	$15.7^{+0.2}_{-0.2}$	$114.7^{+0.0}_{-0.0}$	$100.5^{+0.3}_{-0.3}$	$-180.1^{+0.8}_{-0.8}$	$150.5^{+2.2}_{-2.1}$	$72.9^{+2.1}_{-2.1}$	$167.3^{+2.3}_{-2.4}$	$245.9^{+1.8}_{-1.8}$
Laevens 3	$58.9^{+1.2}_{-1.2}$	$112.3^{+0.0}_{-0.0}$	$251.3^{+0.2}_{-0.2}$	$129.3^{+2.4}_{-2.6}$	$72.2^{+27.4}_{-26.0}$	$-36.6^{+18.0}_{-19.6}$	$83.7^{+25.3}_{-23.9}$	$154.4^{+14.9}_{-11.9}$
Liller 1	$0.7^{+0.0}_{-0.0}$	$89.8^{+0.1}_{-0.0}$	$82.6^{+17.3}_{-15.2}$	$108.8^{+20.1}_{-25.6}$	$-24.9^{+2.3}_{-2.5}$	$52.5^{+24.2}_{-37.3}$	$58.7^{+21.7}_{-23.6}$	$123.7^{+8.9}_{-8.2}$
Mercer 5	$3.2^{+0.3}_{-0.3}$	$89.8^{+0.0}_{-0.0}$	$328.3^{+5.6}_{-7.3}$	$-169.8^{+11.5}_{-7.1}$	$-10.5^{+1.8}_{-1.9}$	$-207.4^{+6.4}_{-9.9}$	$207.6^{+10.2}_{-6.4}$	$268.4^{+2.9}_{-2.8}$
Munoz 1	$47.3^{+1.5}_{-1.5}$	$47.1^{+0.1}_{-0.1}$	$298.5^{+0.4}_{-0.4}$	$21.2^{+6.3}_{-5.8}$	$118.4^{+30.0}_{-29.3}$	$-89.9^{+38.9}_{-37.6}$	$151.5^{+36.0}_{-38.8}$	$153.0^{+35.7}_{-37.7}$
NGC 104	$7.5^{+0.0}_{-0.0}$	$115.1^{+0.1}_{-0.1}$	$22.6^{+0.2}_{-0.1}$	$-8.8^{+0.4}_{-0.3}$	$-46.3^{+0.4}_{-0.4}$	$-176.7^{+0.5}_{-0.5}$	$182.7^{+0.4}_{-0.4}$	$182.9^{+0.3}_{-0.4}$
NGC 1261	$18.2^{+0.1}_{-0.1}$	$135.1^{+0.1}_{-0.1}$	$51.4^{+0.3}_{-0.3}$	$-107.8^{+0.8}_{-0.9}$	$11.2^{+1.7}_{-1.8}$	$32.7^{+2.9}_{-2.7}$	$34.6^{+2.4}_{-2.3}$	$113.2^{+1.5}_{-1.4}$
NGC 1851	$16.6^{+0.1}_{-0.1}$	$114.3^{+0.1}_{-0.1}$	$35.6^{+0.1}_{-0.2}$	$138.8^{+1.0}_{-1.1}$	$28.7^{+1.8}_{-1.9}$	$16.4^{+1.1}_{-1.1}$	$33.1^{+1.7}_{-1.6}$	$142.6^{+1.1}_{-1.2}$
NGC 1904	$19.0^{+0.2}_{-0.1}$	$109.6^{+0.1}_{-0.1}$	$27.8^{+0.1}_{-0.1}$	$48.7^{+0.5}_{-0.5}$	$-22.9^{+2.0}_{-2.1}$	$4.9^{+2.2}_{-2.0}$	$23.4^{+2.5}_{-2.3}$	$54.1^{+0.9}_{-1.0}$
NGC 2298	$15.0^{+0.2}_{-0.1}$	$100.3^{+0.1}_{-0.1}$	$35.6^{+0.3}_{-0.3}$	$-87.4^{+1.2}_{-1.3}$	$-52.5^{+1.7}_{-1.9}$	$28.0^{+3.1}_{-3.1}$	$59.4^{+3.0}_{-2.8}$	$105.6^{+2.8}_{-2.4}$
NGC 2419	$96.0^{+1.7}_{-1.8}$	$66.8^{+0.0}_{-0.0}$	$0.3^{+0.0}_{-0.0}$	$-27.0^{+0.5}_{-0.4}$	$44.7^{+10.5}_{-10.4}$	$-27.0^{+10.3}_{-9.8}$	$53.5^{+10.7}_{-12.6}$	$60.0^{+9.5}_{-10.7}$
NGC 2808	$11.5^{+0.1}_{-0.1}$	$99.7^{+0.0}_{-0.0}$	$57.9^{+0.4}_{-0.3}$	$-148.2^{+0.8}_{-0.8}$	$-5.0^{+0.9}_{-0.9}$	$-26.1^{+1.5}_{-1.5}$	$26.6^{+1.4}_{-1.4}$	$150.6^{+0.6}_{-0.6}$
NGC 288	$12.2^{+0.1}_{-0.1}$	$137.5^{+0.3}_{-0.3}$	$359.7^{+0.0}_{-0.0}$	$-33.4^{+0.6}_{-0.5}$	$-37.6^{+0.5}_{-0.6}$	$61.1^{+3.0}_{-3.5}$	$71.7^{+2.6}_{-2.9}$	$79.1^{+2.3}_{-2.7}$
NGC 3201	$8.9^{+0.0}_{-0.0}$	$85.2^{+0.0}_{-0.0}$	$31.7^{+0.2}_{-0.2}$	$-88.0^{+0.3}_{-0.4}$	$-156.8^{+0.7}_{-0.8}$	$310.4^{+1.0}_{-1.0}$	$347.8^{+1.2}_{-1.2}$	$358.7^{+1.2}_{-1.2}$
NGC 362	$9.6^{+0.1}_{-0.1}$	$131.5^{+0.3}_{-0.3}$	$46.5^{+0.5}_{-0.6}$	$153.9^{+1.9}_{-1.8}$	$-45.2^{+3.7}_{-4.1}$	$7.4^{+1.2}_{-1.3}$	$45.8^{+3.9}_{-3.5}$	$160.6^{+2.8}_{-2.7}$
NGC 4147	$20.7^{+0.1}_{-0.2}$	$29.2^{+0.2}_{-0.1}$	$22.8^{+0.1}_{-0.2}$	$137.2^{+1.0}_{-1.0}$	$-20.3^{+2.9}_{-3.0}$	$7.0^{+2.2}_{-2.2}$	$21.6^{+2.7}_{-2.5}$	$139.0^{+0.6}_{-0.6}$
NGC 4372	$7.2^{+0.0}_{-0.0}$	$97.7^{+0.2}_{-0.2}$	$42.8^{+1.5}_{-1.5}$	$16.7^{+2.4}_{-2.6}$	$-67.3^{+3.0}_{-2.9}$	$-121.7^{+1.6}_{-1.7}$	$139.1^{+2.8}_{-2.8}$	$140.1^{+3.1}_{-3.1}$
NGC 4590	$10.3^{+0.1}_{-0.1}$	$53.5^{+0.1}_{-0.1}$	$61.5^{+0.4}_{-0.3}$	$-120.0^{+0.8}_{-0.7}$	$-109.4^{+1.7}_{-1.6}$	$-283.3^{+0.8}_{-0.9}$	$303.7^{+1.1}_{-1.1}$	$326.5^{+1.0}_{-0.8}$
NGC 4833	$7.1^{+0.0}_{-0.0}$	$97.1^{+0.1}_{-0.1}$	$49.5^{+0.6}_{-0.6}$	$117.9^{+2.5}_{-2.8}$	$27.9^{+0.6}_{-0.6}$	$-29.5^{+2.1}_{-2.0}$	$40.7^{+1.6}_{-1.5}$	$124.6^{+2.9}_{-3.0}$
NGC 5024	$19.0^{+0.1}_{-0.1}$	$16.5^{+0.2}_{-0.2}$	$16.0^{+0.2}_{-0.2}$	$-96.2^{+0.7}_{-0.6}$	$-68.9^{+1.7}_{-1.5}$	$-122.5^{+2.5}_{-2.4}$	$140.5^{+2.2}_{-2.3}$	$170.3^{+1.9}_{-2.1}$
NGC 5053	$18.0^{+0.2}_{-0.2}$	$16.9^{+0.3}_{-0.2}$	$15.3^{+0.2}_{-0.3}$	$8.1^{+0.7}_{-0.7}$	$-93.6^{+1.5}_{-1.4}$	$-120.2^{+2.6}_{-2.7}$	$152.2^{+2.5}_{-2.2}$	$152.5^{+2.4}_{-2.2}$
NGC 5139	$6.5^{+0.0}_{-0.0}$	$77.2^{+0.1}_{-0.1}$	$40.2^{+0.4}_{-0.5}$	$-68.1^{+1.1}_{-1.2}$	$74.3^{+1.5}_{-1.7}$	$87.3^{+0.7}_{-0.8}$	$114.6^{+1.5}_{-1.7}$	$133.3^{+0.8}_{-0.8}$
NGC 5272	$12.1^{+0.1}_{-0.1}$	$34.1^{+0.2}_{-0.2}$	$348.6^{+0.1}_{-0.1}$	$-133.6^{+0.6}_{-0.7}$	$42.5^{+1.1}_{-1.2}$	$-126.3^{+1.1}_{-1.2}$	$133.2^{+1.4}_{-1.3}$	$188.7^{+0.9}_{-0.8}$
NGC 5286	$8.5^{+0.1}_{-0.1}$	$75.9^{+0.0}_{-0.0}$	$83.9^{+0.6}_{-0.6}$	$-195.3^{+0.8}_{-0.8}$	$-57.8^{+1.0}_{-1.1}$	$36.7^{+2.4}_{-2.5}$	$68.5^{+1.7}_{-1.7}$	$207.0^{+0.9}_{-1.0}$
NGC 5466	$16.5^{+0.1}_{-0.1}$	$20.0^{+0.2}_{-0.2}$	$327.2^{+0.4}_{-0.4}$	$265.7^{+0.8}_{-1.0}$	$71.8^{+1.3}_{-1.1}$	$157.6^{+5.4}_{-5.3}$	$173.3^{+5.0}_{-4.9}$	$317.2^{+3.3}_{-3.4}$
NGC 5634	$21.9^{+0.5}_{-0.5}$	$25.9^{+0.3}_{-0.3}$	$147.2^{+0.5}_{-0.6}$	$-39.6^{+0.9}_{-0.8}$	$-22.0^{+2.5}_{-2.6}$	$-55.0^{+5.9}_{-5.7}$	$59.2^{+5.1}_{-5.1}$	$71.3^{+4.0}_{-3.9}$
NGC 5694	$29.2^{+0.5}_{-0.5}$	$52.9^{+0.1}_{-0.1}$	$141.3^{+0.2}_{-0.2}$	$-241.1^{+0.9}_{-0.9}$	$32.6^{+5.4}_{-5.0}$	$32.9^{+4.1}_{-4.1}$	$46.5^{+5.0}_{-4.6}$	$245.6^{+1.8}_{-1.6}$
NGC 5824	$25.5^{+0.5}_{-0.6}$	$62.0^{+0.1}_{-0.1}$	$143.0^{+0.2}_{-0.2}$	$-114.4^{+0.8}_{-0.8}$	$143.5^{+5.4}_{-5.4}$	$-118.3^{+6.9}_{-6.6}$	$185.9^{+7.9}_{-8.1}$	$218.4^{+6.4}_{-6.9}$
NGC 5897	$7.4^{+0.2}_{-0.2}$	$31.4^{+0.6}_{-0.6}$	$125.1^{+1.9}_{-1.9}$	$127.4^{+1.4}_{-1.3}$	$33.9^{+1.4}_{-1.6}$	$-110.7^{+8.9}_{-9.4}$	$115.7^{+8.8}_{-8.0}$	$172.3^{+6.7}_{-6.3}$
NGC 5904	$6.3^{+0.0}_{-0.0}$	$29.0^{+0.5}_{-0.5}$	$353.5^{+0.1}_{-0.1}$	$-299.3^{+1.2}_{-1.1}$	$-165.5^{+3.3}_{-3.4}$	$-111.4^{+0.6}_{-0.7}$	$199.5^{+2.8}_{-2.6}$	$359.7^{+2.3}_{-2.5}$

Downloaded from https://academic.oup.com/mnras/article/519/4/5059/7000207 by guest on 23 April 2024

Table C1 – *continued*

name	R_{GC} (kpc)	θ (deg)	ϕ (deg)	V_r (km s^{-1})	V_θ (km s^{-1})	V_ϕ (km s^{-1})	V_{tan} (km s^{-1})	V_{3D} (km s^{-1})
NGC 5927	$4.8^{+0.0}_{-0.0}$	$81.2^{+0.0}_{-0.0}$	$74.6^{+0.9}_{-0.9}$	$-41.8^{+1.7}_{-1.6}$	$-12.3^{+0.8}_{-0.8}$	$-225.8^{+0.4}_{-0.4}$	$226.2^{+0.4}_{-0.4}$	$230.0^{+0.5}_{-0.4}$
NGC 5946	$5.3^{+0.3}_{-0.3}$	$82.0^{+0.0}_{-0.0}$	$91.5^{+4.1}_{-4.6}$	$51.2^{+8.8}_{-9.8}$	$-93.4^{+3.0}_{-3.2}$	$-12.2^{+9.1}_{-10.4}$	$94.2^{+4.8}_{-3.7}$	$107.2^{+8.6}_{-7.5}$
NGC 5986	$4.9^{+0.1}_{-0.1}$	$59.9^{+0.2}_{-0.2}$	$108.4^{+1.1}_{-1.3}$	$60.4^{+1.8}_{-1.8}$	$50.6^{+1.6}_{-1.7}$	$-36.0^{+4.0}_{-3.7}$	$62.0^{+3.5}_{-3.5}$	$86.5^{+3.7}_{-3.7}$
NGC 6093	$4.0^{+0.1}_{-0.1}$	$29.8^{+0.9}_{-0.9}$	$141.2^{+1.6}_{-1.7}$	$-32.9^{+1.0}_{-1.1}$	$70.0^{+1.9}_{-2.0}$	$-42.5^{+4.2}_{-4.0}$	$81.9^{+3.7}_{-3.7}$	$88.2^{+3.3}_{-3.1}$
NGC 6101	$10.4^{+0.1}_{-0.1}$	$112.2^{+0.0}_{-0.0}$	$103.1^{+0.4}_{-0.4}$	$69.4^{+2.0}_{-2.0}$	$177.3^{+1.5}_{-1.4}$	$304.0^{+1.5}_{-1.3}$	$352.0^{+1.7}_{-1.6}$	$358.8^{+1.7}_{-1.6}$
NGC 6121	$6.4^{+0.0}_{-0.0}$	$85.2^{+0.1}_{-0.1}$	$2.5^{+0.0}_{-0.0}$	$-56.6^{+0.3}_{-0.3}$	$-1.4^{+0.3}_{-0.3}$	$-30.6^{+2.1}_{-2.0}$	$30.7^{+2.0}_{-2.1}$	$64.4^{+1.2}_{-1.2}$
NGC 6139	$3.6^{+0.3}_{-0.3}$	$69.7^{+0.7}_{-0.9}$	$115.6^{+4.3}_{-6.1}$	$54.3^{+1.1}_{-1.5}$	$-120.0^{+5.4}_{-5.0}$	$-82.6^{+10.0}_{-9.3}$	$145.6^{+9.5}_{-9.7}$	$155.5^{+9.1}_{-9.8}$
NGC 6144	$2.5^{+0.0}_{-0.0}$	$27.4^{+0.7}_{-0.5}$	$72.0^{+4.5}_{-4.8}$	$-28.5^{+6.9}_{-8.0}$	$-150.3^{+11.4}_{-11.2}$	$145.1^{+11.1}_{-13.2}$	$208.7^{+0.8}_{-0.9}$	$210.8^{+1.0}_{-1.0}$
NGC 6171	$3.7^{+0.0}_{-0.0}$	$53.1^{+1.1}_{-1.0}$	$354.1^{+0.2}_{-0.2}$	$-35.4^{+1.6}_{-1.5}$	$45.8^{+0.4}_{-0.4}$	$-81.9^{+2.2}_{-2.3}$	$93.8^{+2.1}_{-2.1}$	$100.3^{+1.6}_{-1.5}$
NGC 6205	$8.6^{+0.0}_{-0.0}$	$55.5^{+0.2}_{-0.2}$	$317.4^{+0.4}_{-0.4}$	$-40.3^{+1.2}_{-1.1}$	$66.5^{+1.7}_{-1.7}$	$41.6^{+0.6}_{-0.6}$	$78.5^{+1.2}_{-1.2}$	$88.2^{+0.6}_{-0.6}$
NGC 6218	$4.5^{+0.0}_{-0.0}$	$59.7^{+0.4}_{-0.4}$	$341.5^{+0.3}_{-0.3}$	$-54.5^{+1.1}_{-1.2}$	$67.3^{+0.3}_{-0.3}$	$-112.4^{+1.0}_{-1.0}$	$131.1^{+0.9}_{-1.0}$	$141.9^{+0.6}_{-0.6}$
NGC 6229	$29.5^{+0.4}_{-0.4}$	$48.6^{+0.0}_{-0.0}$	$274.3^{+0.3}_{-0.3}$	$43.5^{+1.0}_{-0.9}$	$-24.3^{+4.9}_{-4.8}$	$-7.9^{+2.6}_{-2.7}$	$25.7^{+4.8}_{-4.9}$	$50.7^{+2.4}_{-2.2}$
NGC 6235	$4.5^{+0.3}_{-0.4}$	$51.3^{+1.8}_{-2.3}$	$176.4^{+0.2}_{-0.3}$	$96.0^{+3.0}_{-3.7}$	$133.1^{+1.8}_{-1.5}$	$-230.9^{+16.3}_{-15.4}$	$266.4^{+13.2}_{-13.1}$	$283.2^{+13.3}_{-13.6}$
NGC 6254	$4.3^{+0.0}_{-0.0}$	$62.2^{+0.5}_{-0.4}$	$341.4^{+0.4}_{-0.4}$	$-60.2^{+0.5}_{-0.6}$	$-86.5^{+0.8}_{-0.8}$	$-103.5^{+1.1}_{-1.2}$	$134.9^{+0.5}_{-0.5}$	$147.7^{+0.6}_{-0.5}$
NGC 6256	$1.9^{+0.1}_{-0.1}$	$76.2^{+1.2}_{-1.0}$	$57.9^{+8.1}_{-7.4}$	$-38.9^{+16.6}_{-16.9}$	$-79.0^{+7.2}_{-8.4}$	$-174.1^{+10.7}_{-7.9}$	$191.3^{+4.3}_{-6.1}$	$195.2^{+1.9}_{-1.9}$
NGC 6266	$2.1^{+0.1}_{-0.1}$	$66.6^{+1.1}_{-1.2}$	$21.5^{+1.3}_{-1.2}$	$72.1^{+0.5}_{-0.5}$	$-37.5^{+0.6}_{-0.6}$	$-114.1^{+1.2}_{-1.3}$	$120.1^{+1.3}_{-1.2}$	$140.1^{+1.2}_{-1.1}$
NGC 6273	$1.5^{+0.0}_{-0.0}$	$18.7^{+1.8}_{-0.6}$	$103.5^{+15.9}_{-20.0}$	$107.6^{+13.6}_{-16.7}$	$-218.2^{+45.7}_{-46.2}$	$174.2^{+40.6}_{-69.5}$	$279.7^{+4.8}_{-4.5}$	$299.6^{+1.1}_{-1.1}$
NGC 6284	$6.4^{+0.4}_{-0.4}$	$67.3^{+0.7}_{-0.8}$	$176.1^{+0.1}_{-0.2}$	$54.3^{+0.7}_{-0.7}$	$-91.3^{+3.8}_{-3.9}$	$3.5^{+6.8}_{-6.0}$	$91.4^{+3.8}_{-3.4}$	$106.3^{+3.2}_{-2.8}$
NGC 6287	$1.6^{+0.1}_{-0.0}$	$16.7^{+11.0}_{-9.8}$	$357.8^{+1.0}_{-4.4}$	$142.9^{+44.1}_{-49.1}$	$266.7^{+25.4}_{-38.7}$	$-62.4^{+30.1}_{-11.7}$	$279.6^{+20.7}_{-26.8}$	$314.4^{+1.1}_{-1.1}$
NGC 6293	$1.5^{+0.3}_{-0.2}$	$33.6^{+8.8}_{-8.1}$	$153.5^{+7.5}_{-11.9}$	$-211.3^{+8.5}_{-2.4}$	$-50.2^{+44.6}_{-40.6}$	$52.7^{+15.0}_{-31.4}$	$73.9^{+19.7}_{-6.4}$	$223.7^{+1.0}_{-0.8}$
NGC 6304	$2.1^{+0.1}_{-0.1}$	$73.7^{+1.1}_{-1.2}$	$12.5^{+1.0}_{-0.9}$	$94.0^{+0.8}_{-0.8}$	$-50.6^{+0.6}_{-0.6}$	$-174.7^{+1.0}_{-0.9}$	$181.9^{+0.9}_{-0.9}$	$204.7^{+1.0}_{-1.1}$
NGC 6316	$3.2^{+0.4}_{-0.4}$	$69.1^{+1.6}_{-2.1}$	$169.5^{+0.9}_{-1.2}$	$129.6^{+1.0}_{-1.2}$	$-49.5^{+7.6}_{-6.6}$	$-96.1^{+14.6}_{-14.1}$	$108.2^{+15.3}_{-16.5}$	$168.8^{+9.5}_{-9.5}$
NGC 6325	$1.3^{+0.2}_{-0.1}$	$32.1^{+11.5}_{-13.1}$	$349.1^{+3.7}_{-9.3}$	$23.2^{+13.6}_{-12.9}$	$-101.1^{+9.6}_{-25.0}$	$178.6^{+6.2}_{-15.8}$	$208.2^{+15.1}_{-16.8}$	$209.4^{+16.8}_{-17.8}$
NGC 6333	$1.8^{+0.0}_{-0.0}$	$26.8^{+0.5}_{-0.1}$	$269.1^{+9.4}_{-9.1}$	$114.0^{+22.0}_{-23.4}$	$79.4^{+41.7}_{-47.0}$	$-326.4^{+23.2}_{-16.1}$	$335.8^{+8.1}_{-9.0}$	$354.8^{+1.8}_{-1.6}$
NGC 6341	$9.8^{+0.0}_{-0.0}$	$60.2^{+0.1}_{-0.1}$	$310.6^{+0.3}_{-0.3}$	$80.4^{+0.6}_{-0.6}$	$-67.0^{+1.5}_{-1.7}$	$0.7^{+1.0}_{-0.9}$	$67.0^{+1.7}_{-1.6}$	$104.7^{+1.1}_{-1.1}$
NGC 6342	$1.6^{+0.0}_{-0.0}$	$28.2^{+3.6}_{-1.8}$	$293.8^{+14.0}_{-18.8}$	$-70.2^{+17.4}_{-15.1}$	$-68.9^{+33.1}_{-15.1}$	$-130.4^{+22.3}_{-23.8}$	$147.8^{+10.7}_{-10.7}$	$163.7^{+3.3}_{-2.6}$
NGC 6352	$3.5^{+0.0}_{-0.0}$	$101.1^{+0.2}_{-0.2}$	$31.1^{+0.7}_{-0.7}$	$45.8^{+1.6}_{-1.7}$	$-14.9^{+0.6}_{-0.5}$	$-213.6^{+1.0}_{-1.0}$	$214.2^{+1.0}_{-1.0}$	$219.0^{+1.2}_{-1.1}$
NGC 6355	$0.9^{+0.1}_{-0.1}$	$18.2^{+14.5}_{-9.7}$	$167.0^{+6.3}_{-18.6}$	$56.5^{+39.0}_{-55.3}$	$-250.7^{+3.4}_{-1.4}$	$69.1^{+20.0}_{-71.8}$	$260.1^{+6.7}_{-12.5}$	$266.3^{+1.2}_{-0.9}$
NGC 6356	$7.9^{+0.9}_{-0.9}$	$69.3^{+1.1}_{-1.3}$	$194.1^{+1.0}_{-0.8}$	$87.4^{+2.0}_{-1.7}$	$-85.0^{+8.2}_{-7.6}$	$-133.6^{+19.8}_{-20.5}$	$158.4^{+21.8}_{-21.0}$	$181.0^{+18.4}_{-17.7}$
NGC 6362	$5.2^{+0.0}_{-0.0}$	$116.3^{+0.2}_{-0.2}$	$63.0^{+0.8}_{-0.8}$	$-18.3^{+0.6}_{-0.6}$	$-102.2^{+1.2}_{-1.2}$	$-118.2^{+0.5}_{-0.5}$	$156.2^{+1.1}_{-1.1}$	$157.3^{+1.1}_{-1.0}$
NGC 6366	$5.2^{+0.0}_{-0.0}$	$79.2^{+0.2}_{-0.2}$	$348.2^{+0.3}_{-0.2}$	$79.2^{+0.5}_{-0.5}$	$78.7^{+0.7}_{-0.8}$	$-118.6^{+1.3}_{-1.3}$	$142.4^{+0.7}_{-0.8}$	$162.9^{+0.9}_{-0.9}$
NGC 6380	$2.1^{+0.2}_{-0.2}$	$104.8^{+1.2}_{-0.9}$	$128.0^{+4.3}_{-7.2}$	$-66.1^{+4.5}_{-6.6}$	$5.9^{+3.4}_{-2.3}$	$23.7^{+1.9}_{-4.0}$	$24.4^{+1.7}_{-2.8}$	$70.5^{+5.3}_{-3.8}$
NGC 6388	$4.0^{+0.1}_{-0.1}$	$108.6^{+0.3}_{-0.3}$	$133.5^{+1.1}_{-1.1}$	$-7.8^{+2.7}_{-2.6}$	$23.1^{+1.3}_{-1.3}$	$80.7^{+1.8}_{-2.0}$	$84.0^{+1.9}_{-2.2}$	$84.4^{+2.2}_{-2.4}$
NGC 6397	$6.0^{+0.0}_{-0.0}$	$94.7^{+0.0}_{-0.0}$	$8.7^{+0.1}_{-0.1}$	$54.9^{+0.7}_{-0.7}$	$126.7^{+0.9}_{-0.9}$	$-102.3^{+0.7}_{-0.7}$	$162.8^{+0.3}_{-0.3}$	$171.9^{+0.5}_{-0.5}$
NGC 6401	$0.8^{+0.0}_{-0.0}$	$40.4^{+2.9}_{-0.7}$	$268.4^{+18.7}_{-20.0}$	$233.0^{+15.1}_{-28.6}$	$90.8^{+15.5}_{-45.9}$	$109.1^{+68.2}_{-77.0}$	$143.9^{+39.6}_{-29.9}$	$273.9^{+1.3}_{-1.4}$
NGC 6402	$4.0^{+0.1}_{-0.1}$	$53.7^{+0.1}_{-0.0}$	$267.6^{+3.6}_{-3.5}$	$-13.9^{+2.4}_{-2.4}$	$-34.6^{+2.7}_{-2.5}$	$-47.2^{+4.2}_{-4.8}$	$58.5^{+5.4}_{-4.9}$	$60.1^{+5.8}_{-5.4}$
NGC 6426	$14.5^{+0.3}_{-0.3}$	$66.3^{+0.2}_{-0.2}$	$224.8^{+0.4}_{-0.4}$	$-123.9^{+1.1}_{-1.2}$	$-23.0^{+2.0}_{-1.9}$	$-106.0^{+6.9}_{-7.0}$	$108.5^{+6.9}_{-6.9}$	$164.6^{+5.5}_{-5.2}$
NGC 6440	$1.2^{+0.1}_{-0.0}$	$62.9^{+0.6}_{-0.2}$	$269.1^{+11.2}_{-10.9}$	$47.7^{+9.6}_{-10.9}$	$67.4^{+3.0}_{-4.7}$	$35.9^{+12.0}_{-15.1}$	$76.3^{+2.8}_{-3.0}$	$90.1^{+3.3}_{-2.8}$
NGC 6441	$4.8^{+0.1}_{-0.2}$	$103.0^{+0.3}_{-0.2}$	$162.3^{+0.3}_{-0.4}$	$26.5^{+0.5}_{-0.5}$	$20.1^{+1.4}_{-1.3}$	$-114.8^{+4.8}_{-4.6}$	$116.5^{+4.7}_{-4.8}$	$119.4^{+4.6}_{-4.7}$
NGC 6453	$2.2^{+0.2}_{-0.2}$	$107.7^{+1.2}_{-1.1}$	$158.5^{+1.6}_{-1.7}$	$-64.8^{+2.7}_{-2.3}$	$166.3^{+2.4}_{-2.2}$	$-34.0^{+1.7}_{-2.1}$	$169.7^{+2.8}_{-2.4}$	$181.7^{+3.1}_{-3.1}$
NGC 6496	$2.8^{+0.1}_{-0.1}$	$125.8^{+0.7}_{-0.7}$	$120.5^{+2.5}_{-2.8}$	$46.0^{+6.5}_{-5.8}$	$23.9^{+5.8}_{-6.5}$	$-273.9^{+6.0}_{-5.6}$	$274.9^{+6.1}_{-6.6}$	$278.8^{+5.2}_{-5.3}$
NGC 6517	$3.2^{+0.2}_{-0.2}$	$70.1^{+0.5}_{-0.3}$	$260.7^{+10.8}_{-6.7}$	$31.6^{+4.6}_{-3.3}$	$45.2^{+1.1}_{-1.1}$	$-41.7^{+1.8}_{-3.9}$	$61.8^{+2.5}_{-1.7}$	$69.1^{+4.1}_{-2.0}$
NGC 6522	$0.9^{+0.2}_{-0.1}$	$123.3^{+9.1}_{-6.7}$	$349.6^{+2.5}_{-4.1}$	$124.7^{+27.0}_{-22.0}$	$134.2^{+10.7}_{-21.0}$	$-81.7^{+6.4}_{-5.7}$	$157.1^{+12.0}_{-21.1}$	$200.8^{+3.0}_{-3.1}$
NGC 6528	$0.7^{+0.1}_{-0.1}$	$139.5^{+11.6}_{-9.4}$	$340.5^{+5.6}_{-11.8}$	$-100.9^{+49.8}_{-33.7}$	$174.9^{+6.7}_{-19.2}$	$-98.7^{+15.8}_{-32.9}$	$204.3^{+15.7}_{-19.8}$	$228.3^{+0.5}_{-0.5}$
NGC 6535	$4.0^{+0.0}_{-0.0}$	$72.9^{+0.4}_{-0.4}$	$311.9^{+1.6}_{-1.7}$	$102.9^{+4.0}_{-4.1}$	$-8.5^{+1.9}_{-1.9}$	$84.1^{+3.6}_{-3.5}$	$84.5^{+3.8}_{-3.7}$	$133.2^{+1.0}_{-0.9}$
NGC 6539	$3.1^{+0.1}_{-0.1}$	$71.3^{+0.5}_{-0.2}$	$279.8^{+7.5}_{-7.1}$	$50.8^{+5.5}_{-6.9}$	$-172.3^{+6.2}_{-6.6}$	$-113.0^{+1.7}_{-2.8}$	$206.0^{+7.2}_{-6.1}$	$212.1^{+8.4}_{-7.5}$
NGC 6540	$2.3^{+0.2}_{-0.3}$	$97.9^{+1.4}_{-1.1}$	$351.5^{+1.2}_{-1.5}$	$6.1^{+0.6}_{-0.6}$	$-61.8^{+2.6}_{-2.8}$	$-120.2^{+5.6}_{-5.5}$	$135.2^{+3.8}_{-3.6}$	$135.4^{+3.8}_{-3.6}$
NGC 6541	$2.2^{+0.0}_{-0.0}$	$132.3^{+0.9}_{-0.9}$	$60.6^{+3.2}_{-3.0}$	$158.6^{+4.2}_{-4.4}$	$7.5^{+4.9}_{-3.6}$	$-200.1^{+5.2}_{-5.6}$	$200.3^{+5.8}_{-5.3}$	$255.5^{+1.9}_{-1.8}$
NGC 6544	$5.6^{+0.1}_{-0.1}$	$90.8^{+0.0}_{-0.0}$	$357.3^{+0.1}_{-0.1}$	$11.9^{+0.7}_{-0.7}$	$77.7^{+2.2}_{-2.0}$	$-22.6^{+5.1}_{-4.6}$	$80.9^{+0.8}_{-0.6}$	$81.8^{+0.7}_{-0.5}$
NGC 6553	$2.9^{+0.1}_{-0.1}$	$95.1^{+0.3}_{-0.3}$	$350.2^{+0.5}_{-0.5}$	$31.0^{+2.2}_{-2.1}$	$3.3^{+0.5}_{-0.5}$	$-232.2^{+0.9}_{-0.9}$	$232.2^{+0.9}_{-0.9}$	$234.3^{+0.7}_{-0.7}$

Downloaded from https://academic.oup.com/mnras/article/519/4/5059/7000207 by guest on 23 April 2024

Table C1 – *continued*

name	R_{GC} (kpc)	θ (deg)	ϕ (deg)	V_r (km s^{-1})	V_θ (km s^{-1})	V_ϕ (km s^{-1})	V_{tan} (km s^{-1})	V_{3D} (km s^{-1})
NGC 6558	$1.0^{+0.2}_{-0.1}$	$138.4^{+12.2}_{-10.0}$	$357.8^{+0.6}_{-1.3}$	$116.2^{+23.1}_{-32.3}$	$-148.5^{+22.6}_{-21.9}$	$-73.7^{+9.3}_{-7.7}$	$165.9^{+16.4}_{-16.2}$	$202.5^{+2.2}_{-2.1}$
NGC 6569	$2.6^{+0.3}_{-0.2}$	$117.3^{+2.2}_{-1.9}$	$182.2^{+0.2}_{-0.2}$	$-47.5^{+0.5}_{-0.5}$	$-1.4^{+2.3}_{-2.2}$	$-179.2^{+10.7}_{-10.8}$	$179.2^{+10.9}_{-10.7}$	$185.4^{+10.5}_{-10.2}$
NGC 6584	$7.0^{+0.1}_{-0.1}$	$123.0^{+0.3}_{-0.3}$	$137.0^{+0.6}_{-0.7}$	$302.7^{+1.5}_{-1.5}$	$87.0^{+3.3}_{-4.0}$	$-121.1^{+7.9}_{-7.4}$	$149.1^{+7.6}_{-8.6}$	$337.5^{+4.3}_{-4.7}$
NGC 6624	$1.2^{+0.0}_{-0.0}$	$158.4^{+1.5}_{-2.4}$	$295.0^{+11.3}_{-13.8}$	$107.9^{+7.1}_{-7.6}$	$60.8^{+11.5}_{-12.3}$	$-56.7^{+2.5}_{-1.6}$	$83.2^{+7.1}_{-7.2}$	$136.4^{+1.4}_{-1.3}$
NGC 6626	$3.0^{+0.1}_{-0.1}$	$99.7^{+0.4}_{-0.4}$	$345.6^{+0.6}_{-0.6}$	$-13.0^{+0.5}_{-0.6}$	$95.2^{+2.0}_{-1.7}$	$-45.8^{+2.6}_{-2.3}$	$105.7^{+0.9}_{-0.8}$	$106.5^{+0.8}_{-0.7}$
NGC 6637	$1.7^{+0.1}_{-0.0}$	$156.6^{+2.3}_{-2.6}$	$203.0^{+3.1}_{-2.7}$	$-56.4^{+4.3}_{-3.9}$	$-75.5^{+6.9}_{-6.2}$	$-97.6^{+1.1}_{-1.4}$	$123.2^{+4.9}_{-4.6}$	$135.4^{+2.9}_{-2.5}$
NGC 6638	$2.3^{+0.2}_{-0.3}$	$121.2^{+3.2}_{-2.1}$	$222.6^{+7.3}_{-4.2}$	$32.7^{+1.3}_{-1.2}$	$-49.4^{+2.6}_{-3.3}$	$-18.1^{+1.4}_{-1.7}$	$52.4^{+3.3}_{-2.1}$	$61.9^{+2.9}_{-2.2}$
NGC 6642	$1.6^{+0.0}_{-0.0}$	$122.6^{+0.2}_{-0.5}$	$276.9^{+6.4}_{-6.0}$	$107.2^{+3.5}_{-4.1}$	$-12.1^{+3.4}_{-2.3}$	$21.4^{+9.9}_{-11.0}$	$24.8^{+7.9}_{-6.6}$	$110.1^{+2.1}_{-2.0}$
NGC 6652	$2.2^{+0.1}_{-0.1}$	$147.4^{+2.8}_{-2.5}$	$192.2^{+1.4}_{-1.1}$	$-168.3^{+0.9}_{-0.7}$	$-41.8^{+9.3}_{-8.7}$	$-28.5^{+5.7}_{-5.1}$	$50.5^{+10.4}_{-10.8}$	$175.9^{+2.9}_{-2.9}$
NGC 6656	$4.9^{+0.0}_{-0.0}$	$94.7^{+0.1}_{-0.1}$	$353.5^{+0.1}_{-0.1}$	$189.9^{+1.1}_{-1.0}$	$133.8^{+1.7}_{-1.7}$	$-181.5^{+0.6}_{-0.5}$	$225.5^{+0.7}_{-0.7}$	$294.8^{+1.1}_{-1.1}$
NGC 6681	$2.3^{+0.1}_{-0.1}$	$151.2^{+2.1}_{-1.9}$	$204.4^{+2.5}_{-1.9}$	$262.2^{+4.0}_{-5.1}$	$-101.2^{+10.1}_{-11.2}$	$-5.9^{+5.6}_{-7.4}$	$101.4^{+11.8}_{-10.3}$	$281.1^{+0.7}_{-0.6}$
NGC 6712	$3.5^{+0.0}_{-0.0}$	$98.7^{+0.2}_{-0.3}$	$294.0^{+4.1}_{-3.7}$	$149.2^{+1.9}_{-2.3}$	$139.8^{+5.1}_{-5.7}$	$11.4^{+8.2}_{-9.7}$	$140.3^{+6.0}_{-6.1}$	$204.8^{+2.7}_{-2.9}$
NGC 6715	$18.6^{+0.3}_{-0.3}$	$110.1^{+0.1}_{-0.1}$	$188.2^{+0.0}_{-0.0}$	$144.0^{+0.4}_{-0.4}$	$-268.5^{+4.1}_{-4.0}$	$-63.8^{+3.8}_{-4.1}$	$276.0^{+4.5}_{-4.7}$	$311.2^{+3.9}_{-4.0}$
NGC 6717	$2.3^{+0.0}_{-0.0}$	$126.5^{+0.7}_{-0.7}$	$299.3^{+2.6}_{-2.7}$	$-20.2^{+1.5}_{-1.5}$	$-17.7^{+1.4}_{-1.4}$	$-100.2^{+1.1}_{-1.1}$	$101.7^{+1.1}_{-0.9}$	$103.7^{+1.2}_{-1.1}$
NGC 6723	$2.4^{+0.0}_{-0.0}$	$174.7^{+1.7}_{-1.6}$	$357.6^{+0.6}_{-1.1}$	$43.6^{+2.2}_{-2.4}$	$-104.8^{+3.0}_{-4.6}$	$-161.6^{+2.6}_{-2.1}$	$192.7^{+0.9}_{-0.9}$	$197.7^{+0.8}_{-1.0}$
NGC 6749	$4.9^{+0.1}_{-0.0}$	$93.1^{+0.1}_{-0.1}$	$293.9^{+2.5}_{-2.4}$	$-30.9^{+2.4}_{-2.5}$	$0.8^{+0.8}_{-0.8}$	$-100.1^{+3.0}_{-3.0}$	$100.1^{+3.0}_{-3.0}$	$104.8^{+3.5}_{-3.5}$
NGC 6752	$5.2^{+0.0}_{-0.0}$	$109.6^{+0.3}_{-0.3}$	$17.4^{+0.3}_{-0.3}$	$-39.9^{+0.7}_{-0.7}$	$-49.7^{+0.2}_{-0.3}$	$-161.4^{+0.9}_{-0.9}$	$168.8^{+0.9}_{-0.8}$	$173.5^{+0.7}_{-0.7}$
NGC 6760	$5.1^{+0.2}_{-0.1}$	$96.1^{+0.1}_{-0.2}$	$285.9^{+4.6}_{-4.1}$	$90.1^{+2.3}_{-3.2}$	$9.8^{+1.2}_{-1.1}$	$-122.3^{+3.9}_{-5.0}$	$122.7^{+5.0}_{-3.8}$	$152.2^{+2.5}_{-2.0}$
NGC 6779	$9.9^{+0.1}_{-0.1}$	$81.1^{+0.0}_{-0.0}$	$290.2^{+0.6}_{-0.6}$	$153.4^{+0.7}_{-0.7}$	$-88.2^{+2.1}_{-2.1}$	$39.2^{+1.8}_{-2.0}$	$96.5^{+2.6}_{-2.6}$	$181.3^{+1.5}_{-1.5}$
NGC 6809	$3.9^{+0.0}_{-0.0}$	$122.0^{+0.6}_{-0.5}$	$347.0^{+0.3}_{-0.3}$	$-140.6^{+1.2}_{-1.1}$	$153.7^{+1.7}_{-1.6}$	$-62.8^{+1.2}_{-1.1}$	$166.0^{+1.2}_{-1.1}$	$217.6^{+0.2}_{-0.2}$
NGC 6838	$6.8^{+0.0}_{-0.0}$	$92.5^{+0.0}_{-0.0}$	$330.7^{+0.4}_{-0.3}$	$32.3^{+0.5}_{-0.4}$	$-40.2^{+0.4}_{-0.4}$	$-188.7^{+0.3}_{-0.4}$	$192.9^{+0.3}_{-0.3}$	$195.6^{+0.3}_{-0.3}$
NGC 6864	$14.3^{+0.4}_{-0.4}$	$128.4^{+0.3}_{-0.3}$	$214.8^{+0.5}_{-0.5}$	$-115.5^{+1.3}_{-1.2}$	$25.7^{+2.2}_{-2.1}$	$-29.2^{+6.9}_{-7.0}$	$39.0^{+6.1}_{-5.8}$	$121.9^{+3.1}_{-2.6}$
NGC 6934	$12.8^{+0.1}_{-0.1}$	$113.3^{+0.0}_{-0.0}$	$265.1^{+0.4}_{-0.4}$	$-328.9^{+1.8}_{-1.7}$	$8.7^{+1.5}_{-1.5}$	$-113.5^{+6.0}_{-6.3}$	$113.8^{+6.3}_{-6.1}$	$348.0^{+3.7}_{-3.6}$
NGC 6981	$12.5^{+0.2}_{-0.1}$	$135.7^{+0.1}_{-0.1}$	$247.5^{+0.4}_{-0.5}$	$-241.1^{+1.5}_{-1.5}$	$2.1^{+2.0}_{-1.8}$	$-2.4^{+2.9}_{-5.1}$	$4.1^{+4.3}_{-2.7}$	$241.2^{+1.5}_{-1.6}$
NGC 7006	$36.7^{+0.4}_{-0.4}$	$110.8^{+0.0}_{-0.0}$	$256.0^{+0.2}_{-0.1}$	$-178.1^{+1.1}_{-1.0}$	$-22.7^{+4.8}_{-4.4}$	$22.7^{+4.6}_{-4.9}$	$32.4^{+5.4}_{-5.6}$	$181.1^{+0.9}_{-0.8}$
NGC 7078	$10.7^{+0.1}_{-0.1}$	$117.1^{+0.1}_{-0.1}$	$295.4^{+0.4}_{-0.3}$	$7.0^{+0.8}_{-0.8}$	$30.3^{+1.3}_{-1.3}$	$-113.1^{+1.2}_{-1.1}$	$117.1^{+1.3}_{-1.4}$	$117.3^{+1.3}_{-1.3}$
NGC 7089	$10.5^{+0.1}_{-0.1}$	$130.4^{+0.1}_{-0.1}$	$288.0^{+0.5}_{-0.5}$	$227.6^{+0.9}_{-0.8}$	$33.5^{+2.0}_{-1.9}$	$28.9^{+2.6}_{-2.4}$	$44.3^{+3.1}_{-2.9}$	$231.8^{+1.4}_{-1.2}$
NGC 7099	$7.3^{+0.0}_{-0.0}$	$147.1^{+0.3}_{-0.3}$	$318.3^{+0.6}_{-0.6}$	$-122.8^{+1.4}_{-1.4}$	$-8.7^{+3.0}_{-3.0}$	$70.9^{+0.9}_{-0.9}$	$71.5^{+0.8}_{-0.7}$	$142.1^{+1.2}_{-1.2}$
NGC 7492	$23.6^{+0.5}_{-0.5}$	$157.8^{+0.1}_{-0.1}$	$280.5^{+1.2}_{-1.1}$	$-98.4^{+0.8}_{-0.8}$	$52.5^{+7.7}_{-7.5}$	$13.6^{+2.4}_{-2.5}$	$54.3^{+7.1}_{-6.9}$	$112.4^{+3.7}_{-3.5}$
Pal 1	$17.4^{+0.2}_{-0.2}$	$77.8^{+0.1}_{-0.1}$	$331.5^{+0.3}_{-0.3}$	$31.2^{+1.0}_{-1.0}$	$32.4^{+1.5}_{-1.4}$	$-200.6^{+1.8}_{-1.6}$	$203.2^{+1.7}_{-1.8}$	$205.6^{+1.6}_{-1.7}$
Pal 10	$7.6^{+0.7}_{-0.6}$	$86.6^{+0.2}_{-0.1}$	$289.9^{+8.0}_{-6.8}$	$-96.5^{+7.1}_{-4.6}$	$-32.0^{+3.4}_{-3.3}$	$-256.6^{+34.7}_{-39.8}$	$258.6^{+39.8}_{-34.9}$	$275.9^{+39.1}_{-35.0}$
Pal 11	$8.7^{+0.4}_{-0.4}$	$115.4^{+0.3}_{-0.3}$	$244.8^{+2.0}_{-1.8}$	$-23.1^{+1.5}_{-1.4}$	$25.3^{+2.3}_{-2.3}$	$-157.7^{+10.9}_{-11.3}$	$159.9^{+11.3}_{-11.1}$	$161.6^{+11.3}_{-11.3}$
Pal 12	$15.3^{+0.3}_{-0.3}$	$153.4^{+0.2}_{-0.2}$	$247.6^{+1.0}_{-1.0}$	$-39.6^{+0.9}_{-0.9}$	$-163.8^{+4.7}_{-4.8}$	$-300.0^{+4.3}_{-4.7}$	$341.7^{+6.1}_{-5.9}$	$344.0^{+6.1}_{-5.9}$
Pal 13	$24.5^{+0.3}_{-0.3}$	$130.4^{+0.1}_{-0.1}$	$292.8^{+0.3}_{-0.3}$	$242.2^{+1.8}_{-1.5}$	$-101.8^{+4.8}_{-4.8}$	$71.0^{+5.8}_{-6.0}$	$124.0^{+5.8}_{-5.7}$	$272.2^{+4.1}_{-3.9}$
Pal 14	$68.7^{+1.1}_{-1.2}$	$43.9^{+0.1}_{-0.1}$	$213.5^{+0.1}_{-0.1}$	$169.8^{+0.7}_{-0.6}$	$-0.3^{+7.6}_{-9.6}$	$-0.0^{+9.1}_{-9.2}$	$9.6^{+10.2}_{-6.4}$	$170.0^{+1.4}_{-0.5}$
Pal 15	$37.4^{+0.9}_{-0.8}$	$60.8^{+0.1}_{-0.1}$	$203.5^{+0.1}_{-0.1}$	$151.8^{+1.6}_{-1.4}$	$30.2^{+6.8}_{-7.2}$	$-13.1^{+6.1}_{-7.2}$	$33.9^{+7.0}_{-7.7}$	$155.7^{+1.5}_{-1.5}$
Pal 2	$34.1^{+0.8}_{-1.3}$	$96.9^{+0.1}_{-0.1}$	$352.8^{+0.1}_{-0.1}$	$-108.4^{+1.0}_{-1.2}$	$4.3^{+3.4}_{-3.1}$	$-6.1^{+7.1}_{-12.7}$	$10.1^{+9.9}_{-6.1}$	$109.1^{+1.9}_{-1.4}$
Pal 3	$98.1^{+2.4}_{-2.1}$	$49.8^{+0.0}_{-0.0}$	$54.7^{+0.1}_{-0.1}$	$-61.0^{+2.0}_{-1.9}$	$-130.8^{+20.6}_{-20.3}$	$-48.8^{+27.0}_{-26.3}$	$141.7^{+22.4}_{-22.9}$	$154.5^{+20.3}_{-21.1}$
Pal 4	$104.1^{+1.7}_{-1.7}$	$22.2^{+0.1}_{-0.1}$	$17.8^{+0.1}_{-0.1}$	$46.6^{+1.3}_{-1.6}$	$-12.7^{+13.6}_{-21.1}$	$11.1^{+18.9}_{-12.9}$	$23.3^{+19.6}_{-16.3}$	$52.2^{+10.1}_{-4.0}$
Pal 5	$17.3^{+0.5}_{-0.5}$	$24.4^{+0.6}_{-0.6}$	$181.8^{+0.1}_{-0.0}$	$-33.2^{+0.8}_{-0.7}$	$-43.5^{+1.9}_{-2.0}$	$-153.9^{+9.7}_{-10.0}$	$159.8^{+9.7}_{-9.4}$	$163.3^{+9.5}_{-9.3}$
Pal 6	$1.0^{+0.4}_{-0.3}$	$75.9^{+4.7}_{-8.9}$	$344.6^{+5.4}_{-11.4}$	$-154.3^{+33.5}_{-13.6}$	$-229.0^{+25.2}_{-33.0}$	$16.1^{+4.4}_{-22.7}$	$230.0^{+32.6}_{-25.3}$	$277.0^{+11.7}_{-11.9}$
Pal 7	$4.3^{+0.1}_{-0.1}$	$83.6^{+0.5}_{-0.4}$	$336.7^{+1.8}_{-1.7}$	$-99.7^{+4.9}_{-5.0}$	$-35.3^{+0.5}_{-0.5}$	$-254.0^{+0.6}_{-0.6}$	$256.4^{+0.6}_{-0.6}$	$275.0^{+2.0}_{-1.8}$
Pal 8	$4.1^{+0.5}_{-0.5}$	$108.6^{+1.5}_{-1.3}$	$224.4^{+5.2}_{-4.1}$	$-8.0^{+2.0}_{-1.5}$	$33.8^{+2.7}_{-2.4}$	$-95.1^{+16.4}_{-16.8}$	$100.9^{+16.8}_{-16.0}$	$101.3^{+16.8}_{-16.1}$
Pyxis	$38.6^{+0.5}_{-0.5}$	$83.3^{+0.0}_{-0.0}$	$69.2^{+0.2}_{-0.2}$	$-207.7^{+0.9}_{-0.9}$	$-184.8^{+6.6}_{-6.4}$	$28.5^{+4.5}_{-4.3}$	$187.1^{+6.4}_{-6.9}$	$279.5^{+4.6}_{-4.8}$
Rup 106	$18.1^{+0.3}_{-0.2}$	$76.5^{+0.0}_{-0.0}$	$97.5^{+0.3}_{-0.3}$	$-214.0^{+0.9}_{-0.9}$	$-83.9^{+2.1}_{-2.3}$	$-90.9^{+2.0}_{-1.9}$	$123.8^{+2.3}_{-2.4}$	$247.2^{+0.7}_{-0.7}$
Segue 3	$27.9^{+0.9}_{-0.8}$	$112.5^{+0.0}_{-0.0}$	$266.5^{+0.5}_{-0.5}$	$-12.2^{+3.6}_{-3.3}$	$-19.4^{+11.9}_{-12.1}$	$-198.7^{+14.8}_{-16.0}$	$200.0^{+16.7}_{-15.0}$	$200.3^{+16.9}_{-15.0}$
Terzan 1	$2.5^{+0.2}_{-0.2}$	$87.1^{+0.2}_{-0.3}$	$5.6^{+0.6}_{-0.5}$	$-68.5^{+1.0}_{-1.1}$	$-4.3^{+1.0}_{-1.1}$	$-80.7^{+5.5}_{-5.4}$	$80.8^{+5.4}_{-5.4}$	$106.0^{+3.8}_{-4.1}$
Terzan 10	$2.3^{+0.4}_{-0.4}$	$97.7^{+1.0}_{-0.8}$	$200.2^{+3.0}_{-2.2}$	$195.2^{+4.6}_{-6.1}$	$-257.4^{+6.6}_{-6.1}$	$-103.0^{+1.9}_{-2.6}$	$277.1^{+6.0}_{-5.3}$	$338.9^{+7.5}_{-8.0}$
Terzan 12	$3.1^{+0.3}_{-0.2}$	$93.0^{+0.5}_{-0.5}$	$346.1^{+2.2}_{-2.0}$	$-101.4^{+1.5}_{-1.2}$	$-95.7^{+5.7}_{-4.4}$	$-144.8^{+3.5}_{-5.4}$	$174.0^{+1.4}_{-1.0}$	$201.3^{+1.7}_{-1.2}$
Terzan 2	$0.8^{+0.2}_{-0.1}$	$63.9^{+5.9}_{-5.3}$	$46.5^{+18.5}_{-13.7}$	$-101.4^{+34.7}_{-22.2}$	$6.0^{+12.3}_{-2.9}$	$96.7^{+25.8}_{-30.5}$	$96.8^{+27.5}_{-30.4}$	$140.4^{+0.9}_{-0.8}$

Downloaded from https://academic.oup.com/mnras/article/519/4/5059/7000207 by guest on 23 April 2024

Table C1 – *continued*

name	R_{GC} (kpc)	θ (deg)	ϕ (deg)	V_r (km s^{-1})	V_θ (km s^{-1})	V_ϕ (km s^{-1})	V_{tan} (km s^{-1})	V_{3D} (km s^{-1})
Terzan 3	$2.5^{+0.0}_{-0.0}$	$59.8^{+1.6}_{-1.3}$	$65.2^{+8.0}_{-7.0}$	$30.2^{+12.5}_{-14.7}$	$-84.0^{+11.6}_{-14.0}$	$-208.5^{+3.8}_{-1.7}$	$224.8^{+2.3}_{-2.5}$	$226.9^{+0.8}_{-0.7}$
Terzan 4	$0.7^{+0.2}_{-0.1}$	$73.0^{+4.4}_{-3.0}$	$54.2^{+23.0}_{-18.2}$	$44.8^{+3.1}_{-9.7}$	$-89.9^{+3.7}_{-5.7}$	$-57.4^{+1.7}_{-1.5}$	$106.7^{+5.6}_{-3.8}$	$115.8^{+2.3}_{-2.4}$
Terzan 5	$1.6^{+0.1}_{-0.1}$	$82.1^{+0.7}_{-0.9}$	$343.8^{+1.5}_{-1.9}$	$70.3^{+0.9}_{-1.0}$	$36.9^{+1.9}_{-2.0}$	$-42.9^{+6.7}_{-6.0}$	$56.6^{+3.8}_{-4.0}$	$90.1^{+3.1}_{-3.0}$
Terzan 6	$0.8^{+0.3}_{-0.3}$	$107.2^{+10.1}_{-5.3}$	$13.0^{+8.9}_{-4.2}$	$-119.2^{+24.4}_{-10.5}$	$16.8^{+8.6}_{-8.4}$	$103.6^{+29.7}_{-22.6}$	$105.1^{+31.0}_{-23.6}$	$158.8^{+6.5}_{-5.9}$
Terzan 7	$16.9^{+0.5}_{-0.5}$	$119.4^{+0.3}_{-0.3}$	$185.3^{+0.1}_{-0.1}$	$131.0^{+0.5}_{-0.5}$	$-300.8^{+5.5}_{-5.8}$	$-65.6^{+6.6}_{-6.5}$	$307.8^{+7.1}_{-6.5}$	$334.5^{+6.4}_{-6.0}$
Terzan 8	$20.5^{+0.4}_{-0.4}$	$123.9^{+0.2}_{-0.2}$	$188.5^{+0.1}_{-0.1}$	$127.6^{+0.5}_{-0.5}$	$-293.7^{+4.7}_{-5.1}$	$-68.7^{+4.7}_{-5.1}$	$301.8^{+5.7}_{-5.5}$	$327.7^{+5.2}_{-4.9}$
Terzan 9	$2.5^{+0.3}_{-0.3}$	$93.9^{+0.9}_{-0.7}$	$351.9^{+1.4}_{-1.8}$	$-80.1^{+0.5}_{-0.5}$	$54.2^{+4.2}_{-4.3}$	$-47.9^{+9.8}_{-10.7}$	$72.7^{+4.4}_{-2.8}$	$108.1^{+2.9}_{-1.6}$
Ton 2	$1.7^{+0.3}_{-0.3}$	$103.4^{+3.8}_{-2.5}$	$42.7^{+18.5}_{-9.4}$	$-2.9^{+41.8}_{-78.0}$	$-172.2^{+7.2}_{-1.9}$	$-227.5^{+4.4}_{-2.5}$	$285.4^{+2.8}_{-7.3}$	$288.2^{+2.8}_{-2.0}$
UKS 1	$7.6^{+0.5}_{-0.4}$	$88.2^{+0.1}_{-0.1}$	$190.6^{+0.3}_{-0.3}$	$89.7^{+2.0}_{-2.0}$	$-32.5^{+6.0}_{-5.9}$	$-22.5^{+8.1}_{-9.7}$	$40.2^{+8.6}_{-8.6}$	$98.4^{+3.8}_{-3.2}$
VVV CL001	$1.1^{+0.5}_{-0.2}$	$82.9^{+2.1}_{-2.5}$	$302.3^{+22.7}_{-82.7}$	$252.8^{+63.3}_{-429.0}$	$-48.6^{+7.1}_{-68.8}$	$185.5^{+97.5}_{-91.6}$	$202.2^{+94.9}_{-98.2}$	$330.3^{+2.6}_{-2.9}$
Whiting 1	$35.1^{+1.0}_{-1.0}$	$139.4^{+0.3}_{-0.3}$	$348.1^{+0.1}_{-0.1}$	$-147.7^{+2.1}_{-2.0}$	$185.5^{+15.0}_{-12.4}$	$-66.9^{+7.2}_{-7.2}$	$197.4^{+14.0}_{-11.1}$	$246.6^{+12.3}_{-10.0}$

Table C2. Orbital properties of globular clusters for Model PNFW.

name	R_{peri} (kpc)	R_{apo} (kpc)	ecc	name	R_{peri} (kpc)	R_{apo} (kpc)	ecc
NGC 104	$5.5^{+0.0}_{-0.0}$	$7.5^{+0.0}_{-0.0}$	$0.15^{+0.0}_{-0.0}$	NGC 6366	$1.9^{+0.0}_{-0.0}$	$5.7^{+0.1}_{-0.0}$	$0.5^{+0.0}_{-0.0}$
NGC 288	$2.8^{+0.1}_{-0.1}$	$12.3^{+0.1}_{-0.1}$	$0.63^{+0.01}_{-0.01}$	Terzan 4	$0.2^{+0.0}_{-0.0}$	$0.7^{+0.2}_{-0.1}$	$0.57^{+0.03}_{-0.03}$
NGC 362	$0.4^{+0.1}_{-0.1}$	$12.6^{+0.2}_{-0.2}$	$0.93^{+0.01}_{-0.01}$	BH 229	$0.9^{+0.1}_{-0.1}$	$1.7^{+0.1}_{-0.1}$	$0.29^{+0.02}_{-0.01}$
Whiting 1	$22.5^{+2.1}_{-1.7}$	$80.1^{+14.5}_{-8.9}$	$0.56^{+0.03}_{-0.01}$	FSR 1758	$3.2^{+0.8}_{-0.8}$	$12.0^{+5.1}_{-3.5}$	$0.58^{+0.04}_{-0.02}$
NGC 1261	$1.3^{+0.2}_{-0.1}$	$21.1^{+0.2}_{-0.2}$	$0.88^{+0.01}_{-0.01}$	NGC 6362	$3.0^{+0.0}_{-0.0}$	$5.2^{+0.0}_{-0.0}$	$0.27^{+0.0}_{-0.0}$
Pal 1	$14.9^{+0.3}_{-0.3}$	$18.9^{+0.4}_{-0.3}$	$0.12^{+0.01}_{-0.0}$	Liller 1	$0.1^{+0.0}_{-0.0}$	$0.8^{+0.1}_{-0.0}$	$0.79^{+0.09}_{-0.09}$
E 1	$12.3^{+23.9}_{-9.3}$	$126.7^{+5.6}_{-3.9}$	$0.82^{+0.13}_{-0.26}$	NGC 6380	$0.2^{+0.0}_{-0.0}$	$2.2^{+0.2}_{-0.2}$	$0.86^{+0.03}_{-0.01}$
Eridanus	$15.9^{+5.4}_{-5.0}$	$144.5^{+8.6}_{-5.9}$	$0.8^{+0.05}_{-0.05}$	Terzan 1	$0.5^{+0.1}_{-0.1}$	$2.6^{+0.2}_{-0.2}$	$0.69^{+0.03}_{-0.03}$
Pal 2	$0.6^{+0.6}_{-0.1}$	$39.9^{+1.0}_{-1.5}$	$0.97^{+0.01}_{-0.03}$	Ton 2	$1.7^{+0.2}_{-0.4}$	$2.9^{+0.5}_{-0.3}$	$0.27^{+0.05}_{-0.01}$
NGC 1851	$1.6^{+0.0}_{-0.0}$	$21.0^{+0.1}_{-0.1}$	$0.86^{+0.0}_{-0.0}$	NGC 6388	$1.0^{+0.0}_{-0.0}$	$4.0^{+0.1}_{-0.1}$	$0.59^{+0.01}_{-0.01}$
NGC 1904	$0.2^{+0.0}_{-0.0}$	$19.6^{+0.2}_{-0.1}$	$0.98^{+0.0}_{-0.0}$	NGC 6402	$0.5^{+0.1}_{-0.1}$	$4.0^{+0.1}_{-0.1}$	$0.77^{+0.02}_{-0.02}$
NGC 2298	$1.6^{+0.1}_{-0.1}$	$16.4^{+0.2}_{-0.2}$	$0.82^{+0.01}_{-0.01}$	NGC 6401	$0.2^{+0.1}_{-0.1}$	$1.5^{+0.1}_{-0.0}$	$0.73^{+0.07}_{-0.1}$
NGC 2419	$13.4^{+4.0}_{-4.1}$	$97.5^{+1.7}_{-1.9}$	$0.76^{+0.07}_{-0.06}$	NGC 6397	$2.5^{+0.0}_{-0.0}$	$6.3^{+0.0}_{-0.0}$	$0.43^{+0.0}_{-0.0}$
Pyxis	$19.9^{+1.0}_{-1.0}$	$142.8^{+12.3}_{-10.9}$	$0.75^{+0.01}_{-0.01}$	Pal 6	$0.6^{+0.1}_{-0.1}$	$1.9^{+0.7}_{-0.8}$	$0.51^{+0.05}_{-0.11}$
NGC 2808	$0.8^{+0.0}_{-0.0}$	$14.6^{+0.1}_{-0.1}$	$0.9^{+0.0}_{-0.0}$	NGC 6426	$4.1^{+0.5}_{-0.4}$	$18.1^{+0.7}_{-0.6}$	$0.63^{+0.02}_{-0.02}$
E 3	$8.9^{+0.2}_{-0.1}$	$13.3^{+1.0}_{-0.9}$	$0.2^{+0.03}_{-0.03}$	Djorg 1	$0.9^{+0.6}_{-0.2}$	$6.8^{+7.1}_{-2.4}$	$0.77^{+0.04}_{-0.05}$
Pal 3	$63.2^{+14.4}_{-16.4}$	$123.7^{+22.1}_{-9.7}$	$0.34^{+0.09}_{-0.03}$	Terzan 5	$0.1^{+0.0}_{-0.0}$	$1.7^{+0.1}_{-0.1}$	$0.85^{+0.02}_{-0.02}$
NGC 3201	$8.4^{+0.0}_{-0.0}$	$33.8^{+0.6}_{-0.5}$	$0.6^{+0.0}_{-0.0}$	NGC 6440	$0.1^{+0.0}_{-0.0}$	$1.3^{+0.0}_{-0.0}$	$0.8^{+0.02}_{-0.02}$
ESO 93-8	$12.4^{+0.9}_{-1.7}$	$13.1^{+2.0}_{-0.6}$	$0.05^{+0.04}_{-0.03}$	NGC 6441	$1.8^{+0.1}_{-0.1}$	$4.9^{+0.1}_{-0.2}$	$0.46^{+0.02}_{-0.02}$
Pal 4	$5.3^{+6.0}_{-3.9}$	$108.9^{+1.9}_{-1.9}$	$0.91^{+0.07}_{-0.09}$	Terzan 6	$0.2^{+0.0}_{-0.0}$	$1.0^{+0.4}_{-0.4}$	$0.66^{+0.09}_{-0.15}$
Crater	$73.8^{+71.9}_{-58.4}$	$148.7^{+55.0}_{-3.7}$	$0.5^{+0.4}_{-0.34}$	NGC 6453	$0.8^{+0.1}_{-0.1}$	$2.4^{+0.2}_{-0.2}$	$0.5^{+0.01}_{-0.01}$
NGC 4147	$1.3^{+0.1}_{-0.1}$	$26.4^{+0.2}_{-0.3}$	$0.91^{+0.01}_{-0.01}$	UKS 1	$0.3^{+0.2}_{-0.1}$	$8.2^{+0.5}_{-0.5}$	$0.93^{+0.03}_{-0.04}$
NGC 4372	$2.8^{+0.1}_{-0.1}$	$7.2^{+0.1}_{-0.1}$	$0.45^{+0.01}_{-0.01}$	VVV CL001	$0.4^{+0.6}_{-0.2}$	$3.3^{+1.5}_{-1.0}$	$0.73^{+0.15}_{-0.19}$
Rup 106	$5.0^{+0.2}_{-0.2}$	$36.9^{+0.6}_{-0.6}$	$0.76^{+0.01}_{-0.01}$	NGC 6496	$2.7^{+0.1}_{-0.1}$	$5.3^{+0.3}_{-0.3}$	$0.32^{+0.01}_{-0.01}$
NGC 4590	$9.1^{+0.1}_{-0.0}$	$33.6^{+0.5}_{-0.5}$	$0.57^{+0.0}_{-0.0}$	Terzan 9	$0.3^{+0.1}_{-0.1}$	$2.7^{+0.4}_{-0.4}$	$0.83^{+0.02}_{-0.04}$
BH 140	$1.9^{+0.1}_{-0.1}$	$10.6^{+0.9}_{-0.7}$	$0.7^{+0.0}_{-0.0}$	Djorg 2	$0.6^{+0.1}_{-0.3}$	$0.8^{+0.2}_{-0.1}$	$0.16^{+0.15}_{-0.04}$
NGC 4833	$0.6^{+0.0}_{-0.0}$	$8.1^{+0.1}_{-0.1}$	$0.86^{+0.01}_{-0.01}$	NGC 6517	$0.3^{+0.0}_{-0.0}$	$3.3^{+0.2}_{-0.2}$	$0.82^{+0.01}_{-0.02}$
NGC 5024	$8.7^{+0.2}_{-0.2}$	$23.2^{+0.2}_{-0.2}$	$0.45^{+0.01}_{-0.01}$	Terzan 10	$1.6^{+0.3}_{-0.3}$	$6.3^{+1.3}_{-1.1}$	$0.59^{+0.01}_{-0.01}$
NGC 5053	$10.8^{+0.2}_{-0.2}$	$18.1^{+0.2}_{-0.2}$	$0.25^{+0.01}_{-0.01}$	NGC 6522	$0.4^{+0.2}_{-0.1}$	$1.1^{+0.2}_{-0.1}$	$0.48^{+0.1}_{-0.08}$
NGC 5139	$2.0^{+0.0}_{-0.0}$	$6.9^{+0.0}_{-0.0}$	$0.55^{+0.01}_{-0.01}$	NGC 6535	$1.0^{+0.1}_{-0.1}$	$4.5^{+0.1}_{-0.1}$	$0.63^{+0.02}_{-0.02}$
NGC 5272	$4.9^{+0.1}_{-0.0}$	$16.4^{+0.1}_{-0.1}$	$0.54^{+0.0}_{-0.0}$	NGC 6528	$0.4^{+0.0}_{-0.0}$	$0.9^{+0.3}_{-0.2}$	$0.38^{+0.13}_{-0.15}$
NGC 5286	$0.7^{+0.1}_{-0.1}$	$12.9^{+0.1}_{-0.1}$	$0.9^{+0.01}_{-0.01}$	NGC 6539	$2.5^{+0.2}_{-0.2}$	$3.4^{+0.2}_{-0.1}$	$0.15^{+0.02}_{-0.01}$
AM 4	$24.3^{+0.8}_{-3.2}$	$40.2^{+45.4}_{-15.3}$	$0.29^{+0.28}_{-0.2}$	NGC 6540	$0.9^{+0.2}_{-0.2}$	$2.3^{+0.2}_{-0.3}$	$0.44^{+0.04}_{-0.03}$
NGC 5466	$6.8^{+0.3}_{-0.3}$	$64.0^{+3.2}_{-2.9}$	$0.81^{+0.0}_{-0.0}$	NGC 6544	$0.2^{+0.1}_{-0.0}$	$5.6^{+0.1}_{-0.1}$	$0.91^{+0.02}_{-0.02}$

Downloaded from https://academic.oup.com/mnras/article/519/4/5059/7000207 by guest on 23 April 2024

Table C2 – *continued*

name	$R_{\rm peri}$ (kpc)	$R_{\rm apo}$ (kpc)	ecc	name	$R_{\rm peri}$ (kpc)	$R_{\rm apo}$ (kpc)	ecc
NGC 5634	$3.3^{+0.5}_{-0.4}$	$22.4^{+0.5}_{-0.5}$	$0.74^{+0.03}_{-0.03}$	NGC 6541	$1.3^{+0.1}_{-0.0}$	$3.8^{+0.0}_{-0.0}$	$0.49^{+0.01}_{-0.01}$
NGC 5694	$2.9^{+0.3}_{-0.3}$	$70.8^{+2.0}_{-2.0}$	$0.92^{+0.01}_{-0.01}$	ESO 280-06	$2.2^{+0.4}_{-0.3}$	$14.1^{+0.7}_{-0.6}$	$0.73^{+0.02}_{-0.03}$
IC 4499	$7.0^{+0.2}_{-0.2}$	$29.9^{+0.6}_{-0.6}$	$0.62^{+0.0}_{-0.0}$	NGC 6553	$2.7^{+0.1}_{-0.1}$	$3.5^{+0.1}_{-0.1}$	$0.12^{+0.01}_{-0.01}$
Munoz 1	$30.9^{+14.0}_{-12.8}$	$48.9^{+5.3}_{-2.1}$	$0.24^{+0.21}_{-0.14}$	NGC 6558	$0.4^{+0.0}_{-0.0}$	$1.3^{+0.4}_{-0.3}$	$0.51^{+0.1}_{-0.13}$
NGC 5824	$16.3^{+1.2}_{-1.2}$	$39.7^{+2.6}_{-2.4}$	$0.42^{+0.01}_{-0.0}$	Pal 7	$3.6^{+0.1}_{-0.1}$	$7.0^{+0.3}_{-0.3}$	$0.32^{+0.01}_{-0.01}$
Pal 5	$10.8^{+1.5}_{-1.3}$	$17.9^{+0.7}_{-0.6}$	$0.25^{+0.04}_{-0.04}$	Terzan 12	$1.6^{+0.2}_{-0.1}$	$3.8^{+0.4}_{-0.3}$	$0.39^{+0.0}_{-0.0}$
NGC 5897	$2.5^{+0.3}_{-0.3}$	$9.5^{+0.4}_{-0.4}$	$0.59^{+0.03}_{-0.03}$	NGC 6569	$1.9^{+0.3}_{-0.3}$	$2.8^{+0.3}_{-0.3}$	$0.19^{+0.03}_{-0.03}$
NGC 5904	$2.7^{+0.0}_{-0.0}$	$28.3^{+0.8}_{-0.8}$	$0.82^{+0.0}_{-0.0}$	BH 261	$1.6^{+0.2}_{-0.2}$	$2.9^{+0.2}_{-0.2}$	$0.31^{+0.06}_{-0.06}$
NGC 5927	$4.2^{+0.0}_{-0.0}$	$5.5^{+0.1}_{-0.1}$	$0.13^{+0.01}_{-0.01}$	NGC 6584	$2.4^{+0.2}_{-0.2}$	$24.8^{+1.5}_{-1.5}$	$0.82^{+0.0}_{-0.0}$
NGC 5946	$0.7^{+0.2}_{-0.1}$	$5.5^{+0.4}_{-0.3}$	$0.76^{+0.02}_{-0.03}$	Mercer 5	$2.0^{+0.1}_{-0.0}$	$5.7^{+0.6}_{-0.5}$	$0.49^{+0.02}_{-0.03}$
BH 176	$12.4^{+1.0}_{-1.0}$	$21.5^{+8.3}_{-5.1}$	$0.27^{+0.11}_{-0.1}$	NGC 6624	$0.2^{+0.0}_{-0.0}$	$1.3^{+0.0}_{-0.0}$	$0.69^{+0.03}_{-0.04}$
NGC 5986	$0.4^{+0.1}_{-0.1}$	$5.1^{+0.1}_{-0.1}$	$0.86^{+0.02}_{-0.02}$	NGC 6626	$0.3^{+0.0}_{-0.0}$	$3.0^{+0.1}_{-0.1}$	$0.8^{+0.01}_{-0.01}$
FSR 1716	$2.4^{+0.2}_{-0.2}$	$5.1^{+0.2}_{-0.1}$	$0.36^{+0.02}_{-0.02}$	NGC 6638	$0.1^{+0.0}_{-0.0}$	$2.3^{+0.2}_{-0.3}$	$0.93^{+0.01}_{-0.01}$
Pal 14	$1.3^{+1.4}_{-0.8}$	$118.6^{+2.7}_{-2.5}$	$0.98^{+0.01}_{-0.02}$	NGC 6637	$0.7^{+0.1}_{-0.1}$	$1.8^{+0.1}_{-0.0}$	$0.42^{+0.04}_{-0.04}$
BH 184	$1.7^{+0.1}_{-0.1}$	$4.6^{+0.1}_{-0.1}$	$0.46^{+0.01}_{-0.02}$	NGC 6642	$0.1^{+0.0}_{-0.0}$	$1.9^{+0.0}_{-0.0}$	$0.91^{+0.03}_{-0.04}$
NGC 6093	$1.4^{+0.1}_{-0.1}$	$4.1^{+0.1}_{-0.1}$	$0.49^{+0.02}_{-0.02}$	NGC 6652	$0.3^{+0.1}_{-0.1}$	$3.0^{+0.1}_{-0.1}$	$0.82^{+0.04}_{-0.04}$
NGC 6121	$0.4^{+0.0}_{-0.0}$	$6.6^{+0.0}_{-0.0}$	$0.88^{+0.01}_{-0.01}$	NGC 6656	$3.0^{+0.0}_{-0.0}$	$9.9^{+0.0}_{-0.0}$	$0.54^{+0.0}_{-0.0}$
NGC 6101	$10.1^{+0.1}_{-0.1}$	$45.7^{+1.6}_{-1.4}$	$0.64^{+0.01}_{-0.01}$	Pal 8	$1.3^{+0.5}_{-0.4}$	$4.1^{+0.6}_{-0.5}$	$0.53^{+0.07}_{-0.07}$
NGC 6144	$2.2^{+0.1}_{-0.1}$	$3.2^{+0.0}_{-0.0}$	$0.19^{+0.02}_{-0.02}$	NGC 6681	$0.4^{+0.1}_{-0.1}$	$5.2^{+0.2}_{-0.2}$	$0.85^{+0.02}_{-0.03}$
NGC 6139	$1.8^{+0.3}_{-0.3}$	$3.8^{+0.3}_{-0.3}$	$0.37^{+0.03}_{-0.03}$	NGC 6712	$1.2^{+0.1}_{-0.1}$	$4.7^{+0.0}_{-0.0}$	$0.6^{+0.02}_{-0.02}$
Terzan 3	$2.3^{+0.1}_{-0.1}$	$2.9^{+0.1}_{-0.0}$	$0.11^{+0.01}_{-0.0}$	NGC 6715	$15.1^{+0.4}_{-0.4}$	$62.6^{+4.4}_{-4.1}$	$0.61^{+0.01}_{-0.01}$
NGC 6171	$1.4^{+0.0}_{-0.0}$	$3.8^{+0.0}_{-0.0}$	$0.45^{+0.01}_{-0.01}$	NGC 6717	$0.9^{+0.0}_{-0.0}$	$2.4^{+0.0}_{-0.0}$	$0.45^{+0.0}_{-0.01}$
ESO 452-11	$0.3^{+0.0}_{-0.0}$	$2.3^{+0.1}_{-0.0}$	$0.76^{+0.02}_{-0.02}$	NGC 6723	$1.9^{+0.0}_{-0.0}$	$2.6^{+0.0}_{-0.0}$	$0.16^{+0.01}_{-0.01}$
NGC 6205	$2.3^{+0.0}_{-0.0}$	$8.8^{+0.0}_{-0.0}$	$0.58^{+0.0}_{-0.0}$	NGC 6749	$1.4^{+0.1}_{-0.1}$	$5.0^{+0.1}_{-0.0}$	$0.57^{+0.01}_{-0.01}$
NGC 6229	$2.2^{+0.3}_{-0.3}$	$30.2^{+0.4}_{-0.4}$	$0.86^{+0.02}_{-0.02}$	NGC 6752	$3.4^{+0.0}_{-0.0}$	$5.4^{+0.0}_{-0.0}$	$0.24^{+0.0}_{-0.0}$
NGC 6218	$2.3^{+0.0}_{-0.0}$	$4.7^{+0.0}_{-0.0}$	$0.35^{+0.0}_{-0.0}$	NGC 6760	$1.8^{+0.1}_{-0.0}$	$5.7^{+0.2}_{-0.2}$	$0.51^{+0.02}_{-0.02}$
FSR 1735	$1.2^{+0.1}_{-0.1}$	$4.0^{+0.3}_{-0.3}$	$0.53^{+0.03}_{-0.05}$	NGC 6779	$1.9^{+0.1}_{-0.1}$	$13.1^{+0.2}_{-0.2}$	$0.74^{+0.01}_{-0.01}$
NGC 6235	$3.9^{+0.4}_{-0.4}$	$9.0^{+1.6}_{-1.4}$	$0.39^{+0.03}_{-0.03}$	Terzan 7	$14.8^{+0.5}_{-0.5}$	$73.8^{+10.2}_{-8.7}$	$0.67^{+0.03}_{-0.03}$
NGC 6254	$1.5^{+0.0}_{-0.0}$	$4.6^{+0.0}_{-0.0}$	$0.5^{+0.0}_{-0.0}$	Pal 10	$6.4^{+1.1}_{-1.1}$	$12.8^{+7.1}_{-3.4}$	$0.33^{+0.12}_{-0.05}$
NGC 6256	$1.3^{+0.2}_{-0.2}$	$2.1^{+0.0}_{-0.0}$	$0.21^{+0.08}_{-0.07}$	Arp 2	$18.4^{+0.4}_{-0.4}$	$73.9^{+6.0}_{-5.1}$	$0.6^{+0.02}_{-0.02}$
Pal 15	$2.0^{+0.7}_{-0.7}$	$52.7^{+1.4}_{-1.2}$	$0.93^{+0.02}_{-0.02}$	NGC 6809	$1.6^{+0.0}_{-0.0}$	$5.8^{+0.0}_{-0.0}$	$0.56^{+0.0}_{-0.01}$
NGC 6266	$0.9^{+0.0}_{-0.0}$	$2.3^{+0.1}_{-0.1}$	$0.45^{+0.01}_{-0.01}$	Terzan 8	$18.0^{+0.4}_{-0.4}$	$92.2^{+9.8}_{-8.6}$	$0.67^{+0.02}_{-0.02}$
NGC 6273	$1.3^{+0.0}_{-0.0}$	$3.4^{+0.1}_{-0.1}$	$0.45^{+0.01}_{-0.02}$	Pal 11	$5.0^{+0.8}_{-0.7}$	$8.8^{+0.5}_{-0.4}$	$0.28^{+0.05}_{-0.05}$
NGC 6284	$1.7^{+0.1}_{-0.1}$	$6.7^{+0.4}_{-0.4}$	$0.59^{+0.0}_{-0.01}$	NGC 6838	$4.7^{+0.0}_{-0.0}$	$7.0^{+0.0}_{-0.0}$	$0.2^{+0.0}_{-0.0}$
NGC 6287	$1.3^{+0.2}_{-0.2}$	$4.6^{+0.2}_{-0.1}$	$0.57^{+0.06}_{-0.05}$	NGC 6864	$0.9^{+0.3}_{-0.3}$	$16.8^{+0.6}_{-0.5}$	$0.9^{+0.03}_{-0.03}$
NGC 6293	$0.2^{+0.1}_{-0.0}$	$2.4^{+0.5}_{-0.3}$	$0.84^{+0.02}_{-0.04}$	NGC 6934	$2.9^{+0.2}_{-0.2}$	$60.5^{+3.6}_{-3.2}$	$0.91^{+0.0}_{-0.0}$
NGC 6304	$1.4^{+0.1}_{-0.1}$	$2.6^{+0.1}_{-0.1}$	$0.3^{+0.0}_{-0.0}$	NGC 6981	$0.3^{+0.0}_{-0.0}$	$25.2^{+0.6}_{-0.4}$	$0.98^{+0.0}_{-0.0}$
NGC 6316	$1.1^{+0.3}_{-0.3}$	$3.9^{+0.5}_{-0.5}$	$0.56^{+0.06}_{-0.05}$	NGC 7006	$2.5^{+0.4}_{-0.4}$	$59.1^{+0.9}_{-0.9}$	$0.92^{+0.01}_{-0.01}$
NGC 6341	$2.1^{+0.0}_{-0.0}$	$10.6^{+0.1}_{-0.0}$	$0.67^{+0.0}_{-0.01}$	Laevens 3	$13.1^{+6.2}_{-4.9}$	$83.0^{+5.8}_{-3.8}$	$0.73^{+0.09}_{-0.09}$
NGC 6325	$1.1^{+0.1}_{-0.1}$	$1.3^{+0.2}_{-0.1}$	$0.07^{+0.1}_{-0.01}$	Segue 3	$26.8^{+1.6}_{-3.5}$	$29.6^{+6.8}_{-2.1}$	$0.08^{+0.07}_{-0.03}$
NGC 6333	$1.6^{+0.0}_{-0.0}$	$6.8^{+0.1}_{-0.1}$	$0.62^{+0.01}_{-0.01}$	NGC 7078	$4.1^{+0.1}_{-0.1}$	$10.7^{+0.1}_{-0.1}$	$0.45^{+0.01}_{-0.01}$
NGC 6342	$0.7^{+0.2}_{-0.1}$	$1.7^{+0.1}_{-0.0}$	$0.42^{+0.09}_{-0.1}$	NGC 7089	$1.3^{+0.1}_{-0.1}$	$19.4^{+0.3}_{-0.3}$	$0.87^{+0.01}_{-0.01}$
NGC 6356	$4.1^{+1.3}_{-1.0}$	$9.1^{+1.4}_{-1.2}$	$0.38^{+0.06}_{-0.06}$	NGC 7099	$1.5^{+0.0}_{-0.0}$	$8.8^{+0.1}_{-0.1}$	$0.71^{+0.0}_{-0.0}$
NGC 6355	$0.8^{+0.2}_{-0.1}$	$1.3^{+0.4}_{-0.1}$	$0.26^{+0.05}_{-0.02}$	Pal 12	$15.1^{+0.3}_{-0.3}$	$73.5^{+8.8}_{-7.4}$	$0.66^{+0.03}_{-0.03}$
NGC 6352	$2.9^{+0.0}_{-0.0}$	$3.9^{+0.1}_{-0.1}$	$0.15^{+0.0}_{-0.0}$	Pal 13	$7.1^{+0.4}_{-0.5}$	$69.4^{+3.2}_{-3.2}$	$0.82^{+0.0}_{-0.0}$
IC 1257	$0.8^{+0.4}_{-0.2}$	$20.0^{+1.2}_{-1.7}$	$0.92^{+0.02}_{-0.04}$	NGC 7492	$2.9^{+0.6}_{-0.5}$	$26.9^{+0.7}_{-0.7}$	$0.81^{+0.03}_{-0.03}$
Terzan 2	$0.2^{+0.0}_{-0.0}$	$0.8^{+0.3}_{-0.2}$	$0.65^{+0.12}_{-0.13}$	–	–	–	–

This paper has been typeset from a TEX/LATEX file prepared by the author.

Downloaded from https://academic.oup.com/mnras/article/519/4/5059/7000207 by guest on 23 April 2024